RSC
Applied Interfaces

ROYAL SOCIETY OF CHEMISTRY

REVIEW

View Article Online
View Journal | View Issue



Cite this: *RSC Appl. Interfaces*, 2025, **2**, 1558

# Research progress in enhanced water production strategies for solar-driven interface evaporation

Hang Su, [a] Shanbin Zhang, [a] Limei Li,[a] Youdong Wang,[ac] Qing Xu,[a] Xiang Li*[b] and Jitian Song*[a]

Received 7th July 2025,
Accepted 28th September 2025

DOI: 10.1039/d5lf00191a

rsc.li/RSCApplInter

Solar-driven interfacial evaporation technology (SDIE) has shown considerable potential in addressing global water scarcity, thanks to its eco-friendly, efficient, and versatile nature. By refining light management, thermal management, and water management within SDIE systems, it is possible to attain high evaporation rates, yet there remains room for improving water production capabilities in practical applications. Against this backdrop, this paper offers an comprehensive review of the latest strategies to enhance water production within SDIE systems. It explores the underlying principles, benefits, limitations, and practical applications of various strategies, including rapid steam condensation, latent heat recovery, and light concentration, and highlights the common challenges encountered by current enhancement strategies. Based on the analysis above, this paper synthesizes the critical research directions necessary for transitioning solar distillation water systems into practical applications, with the aim of offering guiding recommendations for the development of the next generation of SDIE systems.



## 1 Introduction

The issue of global water scarcity is intensifying, particularly in impoverished and arid regions.[1–3] According to a 2021 World Meteorological Organization (WMO) report, more than 2 billion individuals are currently without access to clean water resources, a figure expected to nearly double to 5 billion by 2050.[4] This trend poses not only significant challenges to society but also raises critical questions about environmental sustainability.[5–7] Environmental degradation, including glacier melt and altered precipitation patterns due to global warming, further impacts terrestrial water reserves and river flows, with water scarcity directly endangering the health and well-being of communities.[8–10] In this context, the advancement of desalination technologies has become increasingly critical.[11,12] Presently, desalination technologies are predominantly thermal, such as low-temperature multi-effect distillation (LT-MED)[13,14] and multi-stage flash (MSF),[15] and membrane-based, like reverse osmosis (RO).[16–18] While these methods are industrially utilized, thermal desalination contends with high energy demands, and membrane desalination grapples with frequent maintenance and membrane replacement due to fouling.[19–21] In contrast, solar-driven interfacial evaporation (SDIE), powered by sunlight, presents substantial benefits, including its low-carbon, eco-friendly nature. SDIE focuses heat at the air–water interface through photothermal conversion, efficiently circumventing substantial energy transmission losses and significantly enhancing energy conversion efficiency. This positions it as a leading technology for the sustainable production of potable water.[22] The implementation of SDIE in desalination offers a sustainable solution to the global water crisis and actively supports environmental conservation and climate change mitigation efforts.

Research on SDIE spans various dimensions, including light, heat, and water management. These studies aim to optimize the system's core performance indicators such as light absorption rate, photothermal conversion efficiency, and heat loss, in order to enhance the evaporation rate.[23–27] Recent research achievements have shown that through detailed porous structure design and water state regulation for the evaporator,[28–34] it is possible to significantly reduce the enthalpy of evaporation and potentially surpass the thermodynamic evaporation limit (TEL). Nonetheless, the core objective of SDIE systems is to achieve efficient collection of fresh water. Previous studies have primarily focused on improving evaporation

[a] *Tianjin Key Laboratory of Integrated Design and On-line Monitoring for Light Industry & Food Machinery and Equipment, College of Mechanical Engineering, Tianjin University of Science and Technology, Tianjin, 300222, China. E-mail: songjt@tust.edu.cn*
[b] *Key Laboratory of Safety of Hydrogen Energy Storage and Transportation Equipment for State Market Regulation, Beijing 100029, China*
[c] *Technical Institute of Physics and Chemistry, Chinese Academy of Sciences, Beijing, 100190, China*

performance, with relatively less discussion on strategies to enhance water production. Indeed, the efficiency of freshwater collection is another critical factor. Given that the water production capacity of SDIE systems is influenced by a multitude of factors, including the evaporation flux and vapor-to-water conversion efficiency, effectively converting the enhanced evaporation rate into an actual water production rate presents certain challenges.

Defining and determining key performance indicators is crucial for comparing the evaporation and water collection capabilities of SDIE systems. A critical parameter in this regard is the vapor to water efficiency, alternatively known as the water collection efficiency (WCE). This efficiency is a measure of the SDIE system's ability to condense steam back into liquid water. The formula to express this efficiency is:

$$\eta_{vtw} = \frac{m_{wpr}}{m_{wer}} \quad (1)$$

In the formula, $m_{wpr}$ and $m_{wer}$ represent the water production rate (WPR) and the water evaporation rate (WER) under an open system, respectively.

The solar to water efficiency is used to represent the water production performance of the SDIE system and is defined as:

$$\eta_{stw} = \frac{m_{wpr} h_{fg}}{A_{abs} I_d} \quad (2)$$

$h_{fg}$, $A_{abs}$, and $I_d$ represent the enthalpy of brine, the light absorption area, and the solar radiation intensity, respectively. The above equation can be understood as the gain output ratio (GOR),[35–37] and in this paper, the solar to water efficiency $\eta_{stw}$ is used uniformly.

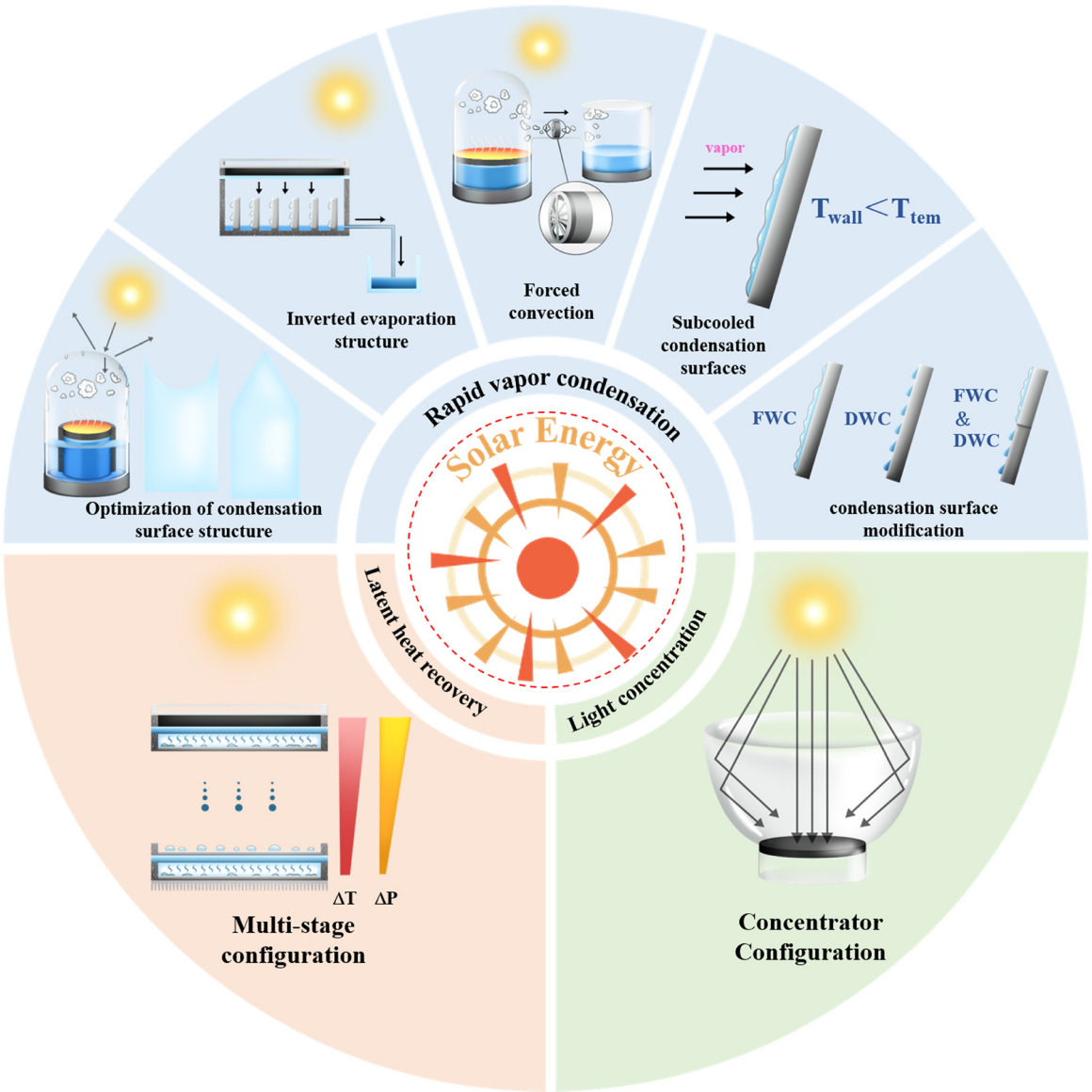


Fig. 1 Enhanced water production strategy in solar-driven interface evaporation.

Over the past decade, SDIE technology has flourished, with numerous reviews published on enhancing water evaporation, yet only a limited number have focused on enhancing water production. This paper offers a systematic review of the diverse strategies used to boost water production and delivers a thorough evaluation of their effectiveness. Recent research has placed greater emphasis on the conversion of evaporation rates into actual freshwater output. By providing a comprehensive assessment of these strategies, this review aims to offer new perspectives for the practical application of SDIE technologies. It begins by exploring strategies designed to expedite vapor condensation, encompassing the optimization of condensation surface structures, the development of inverted evaporation structures, the implementation of forced convection, the creation of subcooled condensation surfaces, and modifications to condensation surfaces as key methodologies (Fig. 1). Furthermore, the paper delves into the latest research progress in latent heat recovery, all-day water production strategies and light concentration technologies, which are pivotal for increasing water production efficiency. Identifying the critical tasks for future enhancement of water production, this article provides invaluable insights and guidance for the practical application of SDIE technology.

# 2 Rapid vapor condensation

Conventional solar-driven interfacial evaporation (SDIE) systems typically feature an enclosed container capped with a transparent cover and equipped with a photothermal component within. The transparent top surface plays a dual role: it transmits solar radiation and facilitates both vapor condensation and the transportation of condensed water. Sunlight passes through the transparent cover, heating the saltwater at the air–water interface and prompting evaporation. The resulting vapor ascends to the top cover, where it condenses into liquid due to the temperature gradient between the environment and the steam, then it flows along the inclined surface to a collection area. These single-stage interfacial evaporation devices, favored for their simplicity and low cost, are well-suited for deployment in remote regions with abundant solar resources to mitigate local water scarcity. Nonetheless, they encounter limitations, including significant light reflection, suboptimal evaporation efficiency, and inadequate water collection.[38–41] These limitations primarily arise from three key factors: firstly, the top surface, often constructed from polymers or glass with high light transmittance and low thermal conductivity, exhibits significant thermal resistance that impacts the vapor condensation efficiency; secondly, the vapor accumulated within the closed system and the condensed water on the transparent top surface reflect incident sunlight, resulting in a reduced light absorption rate of the photothermal material; and lastly, the temperature of the transparent cover that aids condensation rises during extended operation, diminishing the temperature differential and consequently the vapor condensation rate. To mitigate these challenges, strategies such as optimizing the device structure, introducing additional configurations, and harnessing supplementary energy sources can be employed, including adjusting the transparent condensation surface structure, constructing subcooled surfaces, and introducing forced convection. Overall, to enhance water collection efficiency, designers need to conduct a thorough matching of evaporation and condensation capabilities, ensuring that the system is tailored to maximize water production efficiency under various environmental conditions.

### 2.1 Optimization of condensation surface structure

Some small and medium-sized single-stage evaporation devices feature a transparent top cover that serves both light transmission and condensation functions. By altering the geometric structure of the transparent condensation surface, the light absorption rate and water collection efficiency can be significantly enhanced. Typically, the transparent condensation surface is designed with specific angles and curvatures to facilitate the collection of condensed water and the incidence of light. Wang *et al.*[42] designed the first condensation water collection device for interfacial evaporation (Fig. 2a), which uses a partition to separate the device into an evaporation chamber and a condensation chamber. The device is topped with a transparent single-slope cover, and the evaporation chamber bottom has a floating hydrophobic photothermal film that is in contact with seawater. The interfacial water in the evaporation chamber is heated and evaporates, and a solar fan generates airflow to drive the steam towards the condensation chamber. After condensation, the water flows along the single-slope panel in the direction of the tilt until it is collected in the condensation chamber. The experimental results demonstrate that the device has an evaporation rate of 0.92 kg $m^{-2}$ $h^{-1}$ under one sun's intensity. However, during a five-hour outdoor test, the total water production rate is relatively low, at 0.75 kg $m^{-2}$ $d^{-1}$. Designs that utilize a single-slope transparent panel as the condensation surface, such as this one, have been widely adopted by researchers. Nevertheless, the water production efficiency of such designs is quite low and may not meet the daily fresh water requirements for an individual. Considering the dynamic changes in the angle of solar incidence, designers have developed devices with symmetrical condensation surfaces. The symmetrical design allows the condensation surface to absorb incident light at all angles, maintaining a high absorption rate even with large-angle oblique incidence. Moreover, symmetrical condensation surfaces typically have a larger contact area, which enables more effective heat exchange with steam, contributing to improved condensation efficiency. Typical structures include double-slope, conical, hemispherical, concave dome, and pyramidal tops, among others[43–47] (Fig. 2b1–5). In such devices, steam usually condenses on the top surface and then flows along the wall

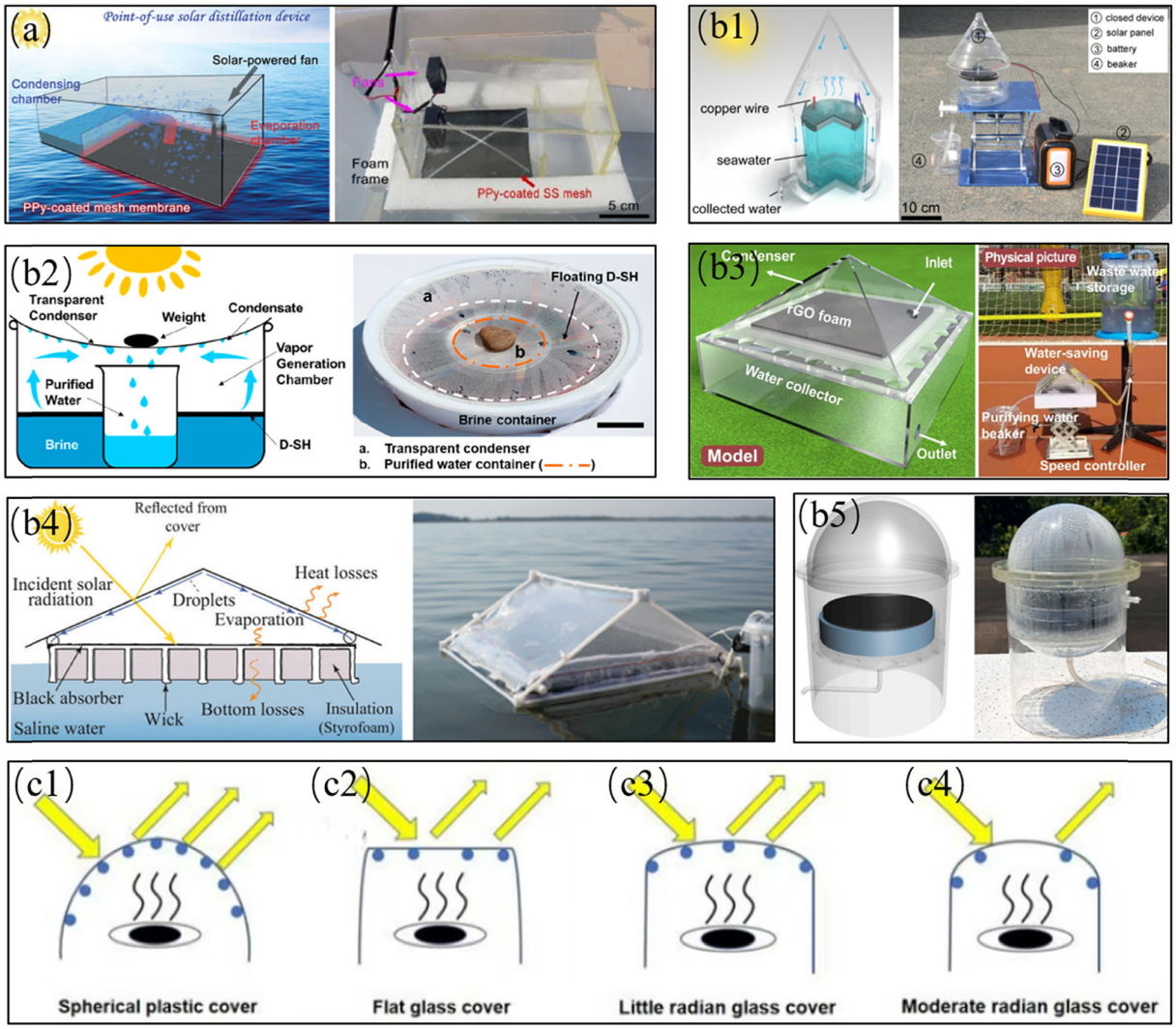


**Fig. 2** a) Single-slope condensation surface seawater desalination interfacial evaporation device;[42] b1) cone-top condensation surface electricity-assisted solar interfacial evaporation device;[43] b2) concave dome condensation surface interfacial evaporation device;[44] b3) pyramid-top condensation surface interfacial evaporation device;[45] b4) double-slope condensation surface interfacial evaporation device;[46] b5) sphere-top condensation surface interfacial evaporation device;[47] c1–4) schematic diagrams of light reflection of different geometrically shaped condensation surfaces.[52]

to the water collection chamber located at the bottom of the device. A typical conical water collection device is shown in Fig. 2b1, where Zhang *et al.*[43] constructed an integrated sealed device with a conical condensation surface using homemade Janus graphene@silicone sponge as the photothermal material. After seawater is heated and evaporates, vapor forms condensate droplets on the conical condensation surface and flows down the conical slope to the annular water storage chamber. In the first two hours of initial evaporation, there are not many droplets on the conical condensation surface. As the evaporation process progresses, the condensation driving force gradually decreases, and a large number of droplets gather on the conical surface. Light reflection further reduces the efficiency of evaporation and water collection. Under the condition of 1 sun illumination with an additional 5 V voltage, the water production rate of the device reached 1.97 kg $m^{-2}$ $h^{-1}$, which is significantly lower than the evaporation rate of 6.53 kg $m^{-2}$ $h^{-1}$ under the same conditions in an open state. Its vapor to water efficiency is only 30.17%, which explains why, despite the device having a very high open evaporation rate, it only produced 9.65 kg $m^{-2}$ of water in a 12 hour outdoor experiment, and even when the outdoor natural light intensity did not reach 1 sun illumination, this water production efficiency is still unsatisfactory. Some SDIE systems with excellent evaporation rates have also shown similar issues in outdoor water production experiments. Despite their theoretical potential for rapid water production, their actual water production capabilities are limited by the low vapor to water efficiency[43–51] (Table 1). The above results indicate that the mismatch between the condensation rate and evaporation rate is a key factor limiting the water

**Table 1** Rapid vapor condensation strategies and performance summary

| Rapid vapor condensation strategy | Photothermal/substrate materials | Indoor evaporation performance (1 sun) | Outdoor water production performance | | Ref. |
|---|---|---|---|---|---|
| | | WER kg $m^{-2}$ $h^{-1}$/vapor to water efficiency %/solar to water efficiency % | Natural light intensity W $m^{-2}$ | WPR kg $m^{-2}$ $d^{-1}$ | |
| — | GO/silicone sponge | 0.92 | — | 0.75 (5 h) | 42 |
| Structural optimization of condensing surfaces | Activated carbon/PVA hydrogel | 6.53/30.17/141 | 40–490 | 9.65 (12 h) | 43 |
| | rGO foam | 2.60 | ~580 | 14.5 (12 h) | 44 |
| | Hydrophilic black cellulose fabric/white cellulose fabric | 2.40 | ~560 | 7.92 (6 h) | 45 |
| | GO hydrogel | 2.10 | ~600 | 0.8 kg $m^{-2}$ $h^{-1}$ | 34 |
| | CB/PVA hydrogel | 0.82 | 0–900 | 2.5 (15 h) | 46 |
| | CB/PVA hydrogel | 3.52 | 0–570 | 9.5 (12 h) | 47 |
| | CNT/chitosan hydrogel | 3.39 | 0–560 | 8.8 (12 h) | 48 |
| | MXene-based aerogel | 1.46/51.37/99.3 | — | — | 92 |
| | CuS-rGO/chitosan-gelatin hydrogel | 3.86 | 400–1150 | 20.6 (8 h) | 51 |
| | CNT/PVA hydrogel | 3.62 | 100–1100 | 25.24 (10 h) | 93 |
| | GO/silicone sponge | 2.09 | 150–800 | 13.0 (11 h) | 94 |
| Inverted evaporation structure + condensation surface modification | TiNOX coated aluminium sheets/hydrophilic fabrics | 1.063/70/51 | 0–866 | 5.4 (12 h) | 53 |
| Inverted evaporation structure | MoC/chitosan hydrogel | 2.19 | 0–890 | 13.68 (9 h) | 54 |
| Inverted evaporation structure + condensation surface modification | Copper foil/chitosan with PVA gel | 2.21/88/132 | 400–600 | 6.5 (5 h) | 55 |
| Forced convection | CB/PVA hydrogel | 3.40 (0.75 m $s^{-1}$)/80/185 | — | — | 60 |
| | GO/PVA hydrogel | 4.18 (40 mL $min^{-1}$)/93.5/266 | 150–800 (natural wind) | 22 (10 h) | 61 |
| | CNT/air-laid paper | 5.55 (5 m $s^{-1}$) | 0–800 (natural wind) | 14.85 (24 h) | 62 |
| | rGo/PVAP | 16.22 (2.5 m $s^{-1}$) | — | — | 63 |
| | CG/chitosan aerogel | 5.98 (6 m $s^{-1}$) | — | — | 66 |
| | Biomass mesoporous carbon/geopolymer | 7.55 (3 m $s^{-1}$) | — | — | 67 |
| | CB/PVA hydrogel | 1.54 (0.6 bar)/92.86/97 | ~840 | 9.5 (7 h) | 68 |
| Subcooled condensing surfaces | λ-$Ti_3O_5$/cellulose membrane | 6.09/52.38/217 | ~820 | 15.3 (6 h) | 29 |
| Forced convection + subcooled condensing surfaces | ppy/PDA sponge | 2.18 | 7.6–7.8 kW h $m^{-2}$ | 15.9–19.4 kg $kW^{-1}$ $h^{-1}$ $m^{-2}$ | 70 |
| Subcooled condensing surfaces + condensation surface modification | SSA/cotton paper | 1.23 | 0–340 | 0.87 | 71 |
| Condensation surface modification | Black TA-$Fe^{3+}$ complex/balsa wood | 1.69/75.7/87 | 300–900 | 8.09 (8 h) | 77 |

collection rate. The different geometric structures of symmetric condensation surfaces also affect the condensation rate of vapor. Que *et al.*[52] conducted a study on the water collection efficiency of solar evaporation devices with different symmetric condensation surfaces (Fig. 2c1–4). Indoor experimental results under the same light intensity show that when using a hemispherical top as the condensation device, the droplets are smallest, but the droplet distribution density is large, and vapor tends to condense on the top surface rather than the side surfaces, thus being more prone to reflect light under vertical illumination. In comparison, when using a flat top or a small-radius hemispherical top, the condensate is more distributed on the side surfaces, and the water collection efficiency is about 38.1% higher than that of the hemispherical top. When using a medium-radius hemispherical top, the device's vapor condensation rate is faster, and the water collection efficiency is further significantly improved, being about 58.8% higher than that of the hemispherical top. It is worth noting that the author's experiments were conducted indoors under vertical light conditions, not under dynamically changing natural light. By changing the geometric structure of the transparent top cover, the light absorption rate and vapor condensation efficiency can be improved, thereby enhancing the water collection rate. In summary, the water production rate is constrained by the evaporation rate and condensation efficiency. Although some advanced photothermal evaporation materials have high evaporation rates, the outdoor water production rate is much lower than the evaporation rate under open conditions due to unresolved key issues such as vapor aggregation, light reflection, and reduced condensation driving force during the evaporation process, which are crucial factors affecting condensation efficiency. Simultaneously increasing the evaporation rate and focusing on enhancing the condensation efficiency of steam, thereby improving the water production capacity,

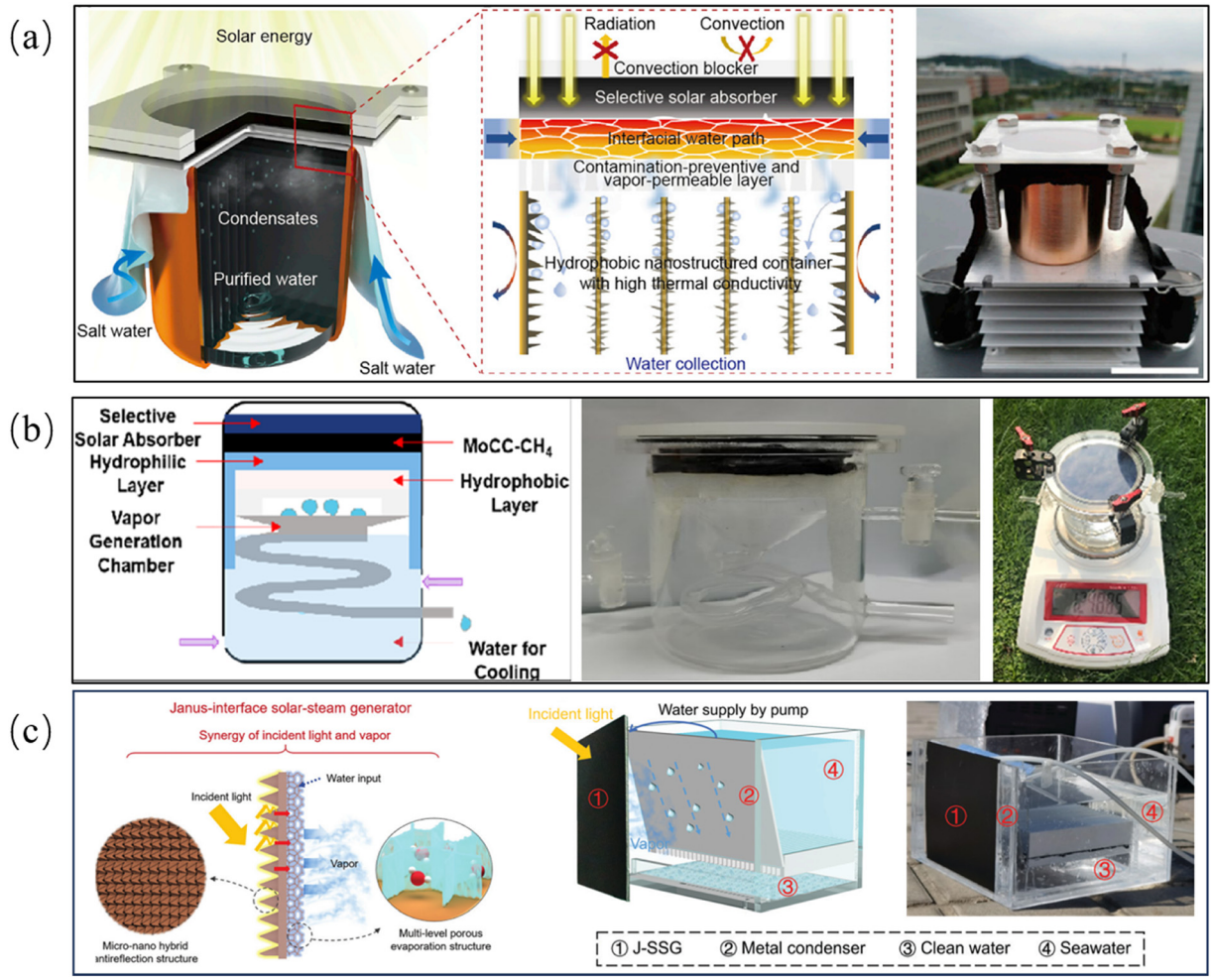


**Fig. 3** a) Solar inverted evaporator with hydrophobic modification of the bottom condensing surface;[53] b) inverted evaporator with condensate tubes at the bottom;[54] c) Janus-interface solar steam generator (J-SSG) surface structure and transfer principle, and evaporator based on the J-SSG integration.[55]

is key to the large-scale promotion and application of SDIE technology.

### 2.2 Inverted evaporation structure

The reversal of vapor flow direction and the construction of an inverted evaporation structure is an effective measure to avoid light loss. As shown in Fig. 3(a), the inverted single-stage solar evaporator device and its schematic diagram designed by Zhu *et al.*[53] consist of a transparent flow restrictor, a photothermal material, a water supply fabric, a porous breathable layer, and a bottom honeycomb-shaped condenser from top to bottom. Sunlight passes through the restrictor and is absorbed by the photothermal material, which converts it into heat energy. This heat energy is transferred downward to the saline water in the water supply fabric, driving the evaporation of water at the interface. The resulting vapor, driven by the pressure gradient, passes through the porous breathable layer downward and finally condenses in the bottom condenser. Compared to traditional solar evaporators, the most significant feature of this device is the reverse flow and condensation of vapor, which avoids light loss. Additionally, the condensation surface of the device has been modified with a hydrophobic nanostructure to enhance the condensation process, and the vapor condensation device at the bottom is made of copper with a high thermal conductivity coefficient, which is more beneficial for the transfer of condensation latent heat to the external environment. This inverted evaporation structure not only avoids light loss caused by vapor condensation but also strengthens the condensation process. Based on this, the device achieves a water production rate of 1.063 kg $m^{-2}$ $h^{-1}$ under one standard sunlight intensity, with a water collection efficiency of up to 70%, producing a total of 5.4 kg $m^{-2}$ of water in a 12 hour outdoor experiment. To further improve condensation efficiency, some studies have assisted vapor condensation through bulk water. As shown in Fig. 3b, the inverted evaporation structure designed by Wang *et al.*[54] uses bulk water stored at the bottom of the device to accelerate vapor condensation, increasing the temperature of

the water to be evaporated and promoting efficient interfacial evaporation, achieving the recovery of vapor latent heat. The design uses a chitosan-based carbon hydrogel as the photothermal material, which not only achieves photothermal conversion but also reduces the evaporation enthalpy of water, accelerating the evaporation rate. A hydrophilic non-woven fabric is used as a continuous water supply channel, and a PVDF membrane is used as a hydrophobic layer to isolate the saline water in the non-woven fabric from the condensed water at the bottom. Due to the pressure difference of vapor on both sides of the hydrophobic membrane, this pressure difference drives the vapor to flow to the bottom condensation tube, where it undergoes heat exchange with the bulk water outside the tube and condenses into water. The latent heat released during the condensation process is used to heat the bulk water for evaporation. Experimental results show that the open evaporation rate of the device under one sunlight intensity is 2.19 kg $m^{-2}$ $h^{-1}$, and the fresh water collection capacity reaches 13.86 kg $m^{-2}$ in a 9 hour outdoor experiment from 8:00 to 17:00 during the day. It should be noted that as the vapor condensation process progresses, the gradual release of latent heat will inevitably cause the temperature of the bulk water to rise and the condensation temperature difference to decrease. Therefore, using the bulk water to be evaporated to promote condensation should ensure sufficient condensation area or enough bulk water. Qu *et al.*[55] leveraged Janus-interface engineering to design a structure with lateral vapor flow, which exhibits an impressive vapor to water efficiency (Fig. 3c). The most notable feature of this design is the construction of a Janus-interface solar-steam generator (J-SSG), with the photothermal side and the evaporation side distributed on opposite sides of the J-SSG. The J-SSG is skeletonized by copper foil/foam, where the copper foil side acts as the photothermal side, and its surface is processed into a pyramid-shaped micro–nano hybrid structure using rapid laser processing to enhance light absorption; the copper foam side is composed of a porous evaporation side made of a mixed membrane of chitosan and PVA aerogel. The team then constructed a seawater desalination water production system to verify the feasibility of the J-SSG material. The J-SSG is placed vertically, with the photothermal side facing outward to absorb light and the evaporation side facing inward for water supply and evaporation. The system includes a water tank for storing seawater, and the evaporation side continuously absorbs water from the tank. On the evaporation side, an inclined condensation surface made of ultra-hydrophobic metal is set up, and the other side of the inclined condensation surface is in contact with a large amount of seawater to accelerate vapor condensation. The condensed water flows along the inclined condensation surface and is ultimately stored in a water collection chamber. Thanks to the high light absorption rate, low-loss photothermal conversion capability, and excellent condensation ability, the system achieves an open evaporation rate of 2.21 kg $m^{-2}$ $h^{-1}$, a water production rate of 1.95 kg $m^{-2}$ $h^{-1}$, and a vapor to water efficiency of 88%, producing a total of 6.5 kg $m^{-2}$ of water in a 5 hour outdoor experiment from 10:00 to 15:00. The team's dual-interface design and multiple strategies to promote vapor condensation significantly enhance the system's evaporation and vapor to water efficiency.

The inverted evaporation structure, which separates the evaporation and condensation surfaces, is an excellent strategy to avoid interference between incident light and condensed water with vapor by keeping them in different areas. With this design approach, the vapor to water efficiency is significantly improved compared to traditional designs. The vapor to water conversion efficiencies in ref. 53 and 55 reached 70% and 88%, respectively, compared to the high open evaporation rate of traditional solar interfacial evaporation devices, which is only 30.17%.[43] The inverted evaporation structure has excellent water collection efficiency, and in future work, more consideration can be given to designing three-dimensional structure evaporators to enhance the evaporation rate. Furthermore, by widely applying photothermal materials in the inverted structure that can reduce the evaporation enthalpy by forming intermediate water or promoting the evaporation of clustered water molecules, the evaporation rate can be increased, thereby enhancing water production capacity.

### 2.3 Forced convection

In recent years, numerous studies have confirmed that introducing a forced convection mechanism into closed solar evaporation systems can significantly enhance the evaporation rate and water collection efficiency. The principles underlying this improvement can be summarized in three key points: firstly, as dictated by classical gas dynamics, the rate of evaporation is governed by two sequential processes: phase transition and vapor diffusion.[56] Although previous research has predominantly concentrated on enhancing the phase transition rate by reducing the enthalpy of evaporation and optimizing the management of light, heat, and water, the influence of vapor diffusion on the rate of evaporation has been largely overlooked. In reality, resistance to vapor diffusion could be a critical factor constraining the evaporation rate. By employing forced convection to stimulate the movement of vapor, the pressure and humidity at the evaporation interface can be reduced, leading to a marked increase in the evaporation rate.[57,58] Secondly, forced convection is capable of directing the vapor accumulated within the evaporation chamber towards the condensation area in a controlled flow. This not only expedites the interaction between the vapor and the condensation surface, thereby promoting the condensation process, but also separates the evaporation and condensation. This separation prevents the light reflection issues that can arise from the aggregation and condensation of vapor within the evaporation chamber. Thirdly, when

rapidly moving air encounters slow-moving vapor, forced convection is initiated, imparting momentum to the vapor. Based on thermal boundary layer theory, increasing the velocity of the vapor flow helps to reduce the thermal boundary layer between the vapor and the condensation surface, which in turn intensifies the heat transfer during condensation.[59] Moreover, the flowing fluid can expedite the shedding of droplets from the condensation surface, increasing the contact area between the vapor and the condensation plate and facilitating rapid condensation.

Yu *et al.*[60] devised an air-assisted SDIE system where the airflow passage is confined between the transparent glass panel and the photothermal material's evaporative surface (Fig. 4a). By manipulating the airflow velocity, the team explored the interplay between evaporation and water production rates. Their research identified an optimal airflow speed; achieving a peak water production rate of 2.7 kg $m^{-2}$ $h^{-1}$ and an impressive vapor to water efficiency of 80% when the airflow was set at 0.75 m $s^{-1}$, coupled with additional cooled water to expedite condensation. This underscores the potency of forced convection in reinforcing steam condensation.

In the SDIE system designed by Zong *et al.*[61] (Fig. 4b), a hydrogel was used as the photothermal material, achieving an open evaporation rate of 4.18 kg $m^{-2}$ $h^{-1}$ under one sun intensity.

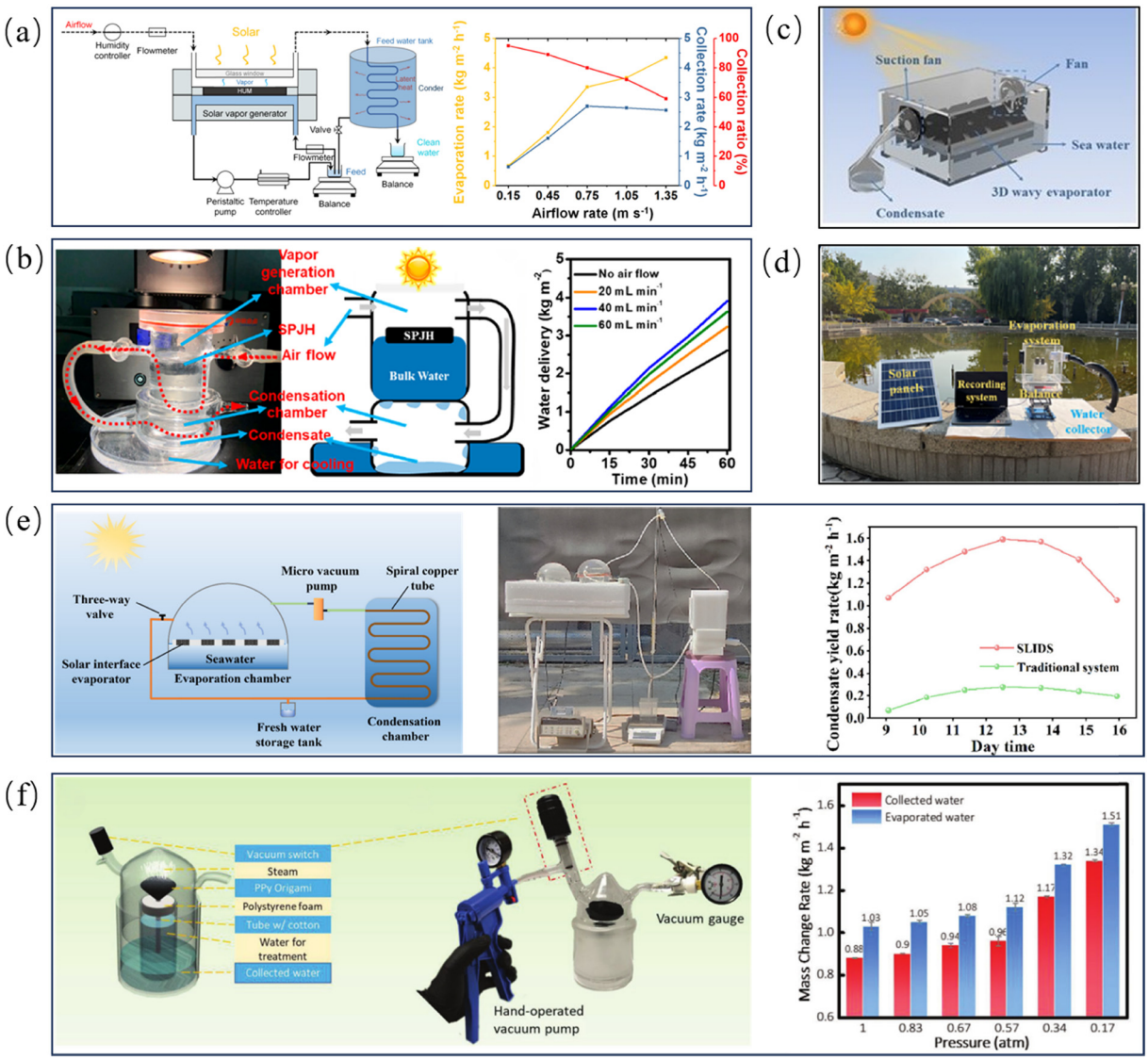


**Fig. 4** a) Schematic diagram of the airflow-enhanced HUM solar interfacial evaporation device, and the evaporation and water collection performance under different airflow conditions;[60] b) principle and device diagram of the SPJH-based solar interfacial evaporator, and the water collection performance of the device under different airflow conditions;[61] c) schematic diagram of the 3D wavy evaporator enhanced by using a fan;[62] d) 3D hydrogel-based outdoor evaporation system enhanced by using a fan;[63] e) schematic diagram of the SLIDS low-pressure evaporation system, the outdoor experimental water collection device and the water collection performance;[68] f) principle and physical diagram of the low-pressure solar water collection system, and the evaporation and water collection performance under different pressures.[69]

However, within a closed system, the water production rate was comparatively modest at 2.60 kg $m^{-2}$ $h^{-1}$. To mitigate this, the study introduced horizontally flowing air into the evaporation chamber to diminish the hydrogel's surface humidity. With an airflow assistance of 40 mL $min^{-1}$, the water production rate was boosted to 3.91 kg $m^{-2}$ $h^{-1}$, and the freshwater collection efficiency saw a significant rise from 62.2% to 93.5%. Hu[62] and Yan[63] enhanced the evaporation and water production performance of a three-dimensional evaporator through the introduction of forced convection, as depicted in Fig. 4c and d. Both studies highlighted that, beyond the effects mentioned, forced convection also fosters the "evaporation cooling" effect in evaporators. This phenomenon can lower the evaporator's surface temperature below the ambient level, enabling the photothermal material to harness additional energy from the surroundings and thus increasing the evaporation rate. For further insights into similar findings, refer to other studies.[56,57,64–67] Researchers have also explored interfacial evaporation processes under low-pressure conditions. Liu[68] designed a low-vacuum solar evaporation system, as illustrated in Fig. 4e, where the evaporator floats within the chamber, and vapor is guided into a spiral pipe condenser by a vacuum pump for condensation. This design prevents vapor condensation within the evaporation chamber and concurrently reduces internal humidity. Experimental outcomes revealed that the incorporation of low-vacuum conditions enhanced the water collection efficiency of this device by 41.6%, with a water production capacity of 9.5 kg $m^{-2}$ achieved during a continuous 7 hour outdoor test. It has been demonstrated that under vacuum conditions, even in the absence of induced forced convection, the decrease in pressure propels the phase change of water molecules to vapor, thereby accelerating evaporation and water production rates. Fan *et al.*[69] validated this using an enclosed solar evaporation device with adjustable vacuum levels, as shown in Fig. 4f. When the device's pressure was regulated to approximately 0.17 atm, the water collection efficiency improved by 52% under ambient pressure conditions.

While the aforementioned studies have convincingly showcased the potential of forced convection in boosting the efficiency of water collection, the majority have not yet undertaken a comprehensive evaluation of the additional investments or operational expenses that come with implementing forced convection—such as the cost of acquiring extra solar photovoltaic components and fans, or the electricity required to directly power fans or vacuum pumps. Consequently, when considering the introduction of additional energy sources, it is imperative to develop and advocate for appropriate methods of assessing energy consumption, given the necessity of considering energy return on investment. The act of introducing more energy without taking into account operational costs, in an effort to enhance the solar evaporation and water production process indefinitely, is counterproductive. Moreover, the possibility of harnessing the abundant and complimentary wind resources from nature should not be overlooked. Establishing criteria for assessing energy consumption will facilitate the comparison of various water collection strategies within this domain. For large-scale industrial seawater desalination, a rational assessment of energy consumption is also more beneficial for comparing SDIE technology with other desalination methods, thereby underscoring its advantages and fostering its commercialization.

### 2.4 Subcooled condensation surface

As the evaporation process proceeds, the temperature differential between the condensation surface and the vapor diminishes, resulting in a weakened condensation driving force for the vapor and consequently a decrease in vapor to water efficiency. To counteract this challenge, the implementation of a subcooled surface to bolster vapor condensation proves to be an effective strategy for enhancing the efficiency of water collection.

To enhance condensation efficiency, Zuo *et al.*[29] incorporated a subcooled condensation surface below ambient temperature within a single-slope condensation surface evaporation device (Fig. 5a). This surface was circulated with cooling water at approximately 10 °C to intensify vapor condensation. Under one sun's intensity, the device registered an open evaporation rate of 6.09 kg $m^{-2}$ $h^{-}1$, while the closed system yielded a water production rate of 3.19 kg $m^{-2}$ $h^{-1}$, with a vapor-to-water conversion efficiency of about 52.38%. During outdoor experiments, with an average sunlight intensity of 820 W $m^{-2}$ over a 12 hour period, the water output reached 15.3 kg $m^{-2}$ $h^{-1}$. Although this exceeded the water collection efficiency of traditional single-stage evaporators without enhanced condensation measures, the improvement was not markedly significant. Studies have demonstrated that forced convection and subcooled surfaces synergistically accelerate vapor condensation. Cheng's team[70] leveraged both forced convection and subcooled surfaces to strengthen vapor condensation (Fig. 5b). In their single-slope condensation surface evaporation device, a baffle separated the evaporation and condensation chambers, with a fan installed to direct vapor to the condensation chamber. A low-temperature condensation plate was installed inside, powered by solar photovoltaic panels. The team's findings indicated that using the condenser alone, without the fan, had minimal impact on the system's water collection efficiency, resulting in a low water production rate of 1.7 to 2.8 kg $m^{-2}$, primarily due to the substantial mass transfer distance between the vapor and the condensation chamber, hindering rapid vapor diffusion to the condenser. Utilizing the fan without the condenser increased the water production rate to 3.2 to 3.9 kg $m^{-2}$, aligning with high evaporation rates under forced convection conditions. However, when both the fan and the condensation plate were employed together, the humidity in the condensation chamber could be swiftly reduced, substantially enhancing the water production rate to 5.1 to

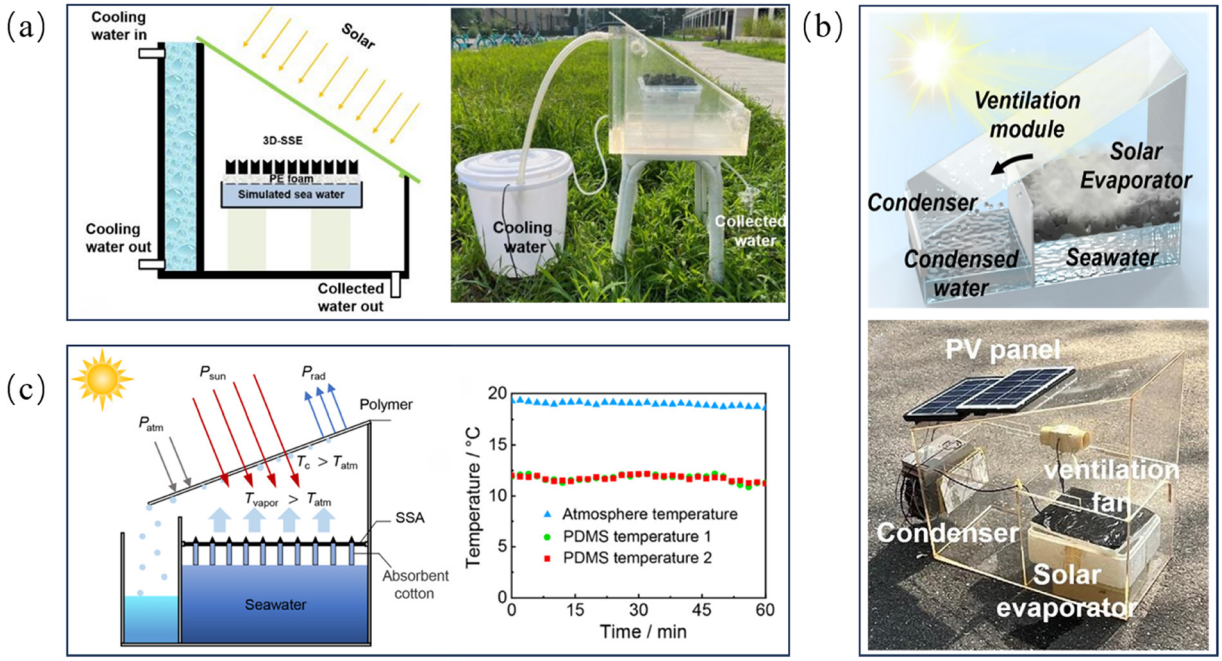


**Fig. 5** a) Schematic and outdoor physical view of a single slope condensing surface evaporation unit with cooling water passed through the sidewalls;[29] b) schematic and outdoor physical view of a single slope condensing surface evaporation unit synergistically enhanced by forced convection and subcooled surfaces;[70] c) schematic of a radiatively-cooled PDMS-based membrane used to build process surfaces and their subcooled temperatures under outdoor conditions.[71]

6.8 kg $m^{-2}$. Importantly, to compare the outdoor water production performance of the device under varying solar total fluxes, the study introduced a new metric, NWPR (kg $kW^{-1}$ $h^{-1}$ $m^{-2}$), representing the water production per square meter of evaporation surface under equal solar input. The designed NWPR achieved 15.9 to 19.4 kg $kW^{-1}$ $h^{-1}$ $m^{-2}$. Radiative cooling technology is also employed to create subcooled surfaces. Chen *et al.*[71] utilized a transparent radiative polymer (PDMS film) as the vapor condensation surface for an all-weather water production device (see Fig. 5c). Thanks to the radiative cooling effect, the PDMS film could attain a subcooled temperature approximately 7 °C below ambient temperature, enhancing condensation and dew collection,[72] with an outdoor water production of 0.87 kg $d^{-1}$. While constructing condensation surfaces is straightforward and somewhat effective, its contribution to improving water collection efficiency is limited. Combining this method with other strategies could potentially achieve superior actual water production performance under fluctuating environmental conditions. Recent research indicates that a lower condensation temperature does not invariably translate to higher condensation efficiency. Although reducing the condensation temperature can decrease the overall system temperature and direct energy loss to the environment, it also amplifies the temperature difference between the evaporation surface and the condensation surface, leading to increased internal heat transfer losses. Appropriately raising the condensation surface temperature can actually improve condensation efficiency.[73] Therefore, when designing subcooled surfaces, it is essential to meticulously consider the cooling system's configuration based on the device's specific structure and operational conditions to optimize water production performance.

### 2.5 Condensation surface modification

When vapor encounters a surface, the surface's structure and free energy can influence the condensation patterns of droplets.[74–76] On hydrophilic surfaces, vapor is more prone to nucleate, and as droplets grow, they tend to spread into a film along the solid surface, a phenomenon referred to as film-wise condensation (FWC), as depicted in Fig. 6a1 and c1. Wang *et al.*[77] leveraged the tendency of vapor to nucleate on hydrophilic surfaces by employing a hydrophilic-modified aluminum plate as the condensation surface (as shown in Fig. 6b). Their research revealed that the water collection efficiency of the hydrophilic aluminum plate outperformed that of the unmodified and hydrophobic-modified aluminum plates by 1.5 and 1.8 times, respectively. Under one sun's intensity, the device achieved a water production rate of approximately 1.28 kg $m^{-2}$ $h^{-1}$, with a water collection efficiency reaching up to 75.7%. Over an 8 hour outdoor experiment from 9:00 to 17:00, a total of 8.09 kg $m^{-2}$ of water was produced, showcasing excellent water production performance. Xu's team[78] coated PET plastic with a superhydrophilic layer for the condensation surface during the solar interfacial evaporation process. While the uncoated PET surface became blurry within 30 minutes (Fig. 6d1), the superhydrophilic coated PET surface remained transparent

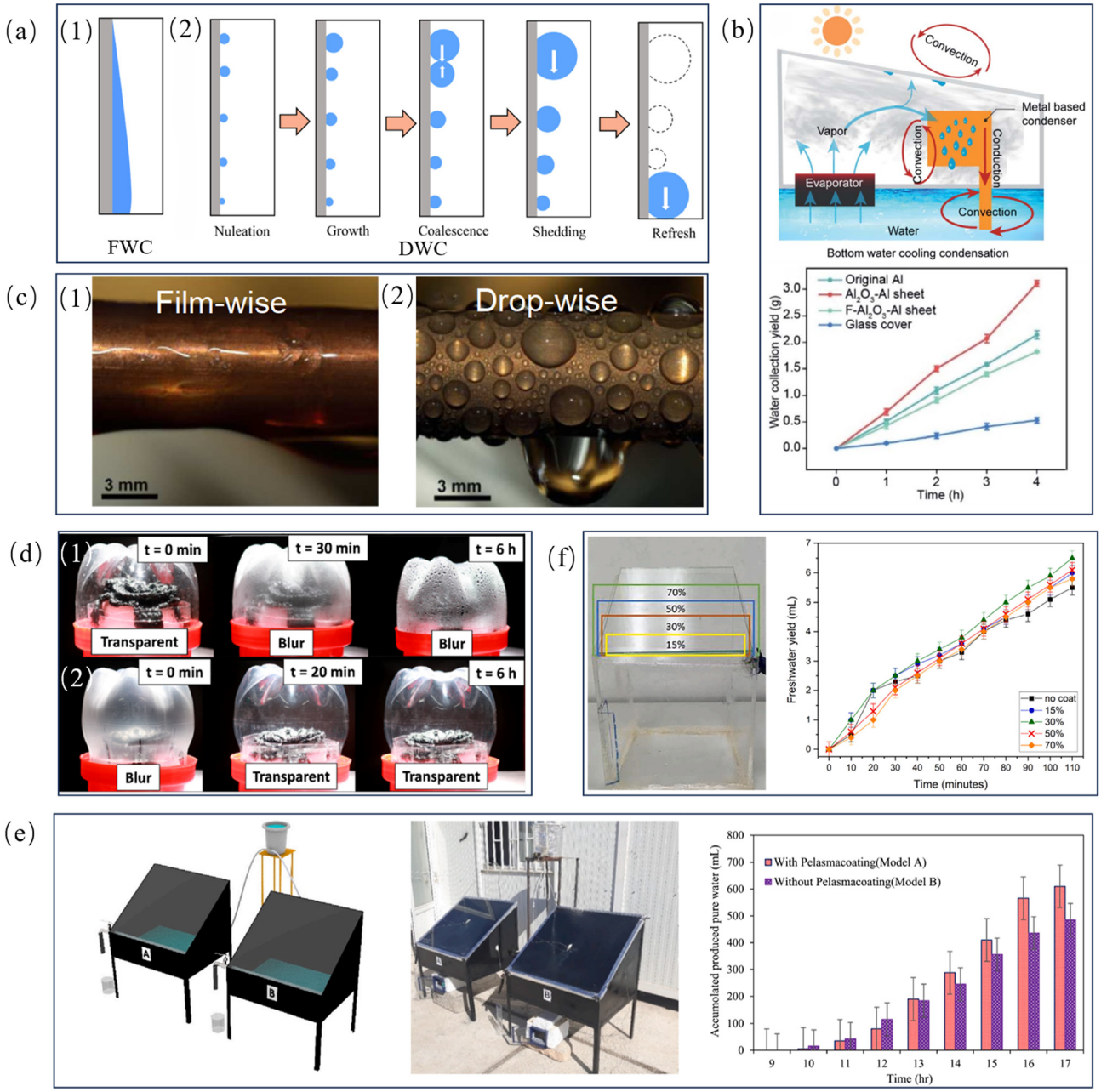


**Fig. 6** a) Schematic diagrams of film-wise condensation and drop-wise condensation;[75] b) hydrophilic modified aluminum plate used for the solar evaporation device;[77] c) vapor condensation morphology on hydrophilic *versus* hydrophobic surfaces;[91] d1 and 2) laws of change of surface hydrophobically modified *versus* unmodified PET condensation surfaces with the evaporation process;[78] e) experimental setup diagrams of hydrophobically modified surface *versus* unmodified glass cover plate used for condensation;[81] f) law of the effect of different hydrophobically modified areas on the amount of water collected.[82]

for 6 hours (Fig. 6d2), with a vapor-to-water conversion efficiency that was about 37% higher. Although hydrophilic condensation surfaces can facilitate vapor condensation, once a liquid film covers the condensation surface, the thermal resistance increases, which is detrimental to condensation during extended solar evaporation processes.[79,80] Consequently, current research favors modifying the condensation surface to be hydrophobic. On hydrophobic surfaces, vapor condensation tends to form droplets rather than a film, known as drop-wise condensation (DWC), as illustrated in Fig. 6a2 and c2. DWC primarily involves four steps: nucleation, growth, coalescence, and sliding of droplets. DWC mode features a slower nucleation rate, but once droplets coalesce into larger droplets, they are more likely to slide off the surface, refreshing the condensation surface for the subsequent condensation cycle and thus enhancing condensation efficiency. There are currently two main methods to achieve DWC mode: one is to

use low surface energy coatings, and the other is to create micro–nano scale surface features.[75] As mentioned in a previous literature report,[53] a hydrophobic surface was constructed by creating micro–nano scale features on the condensation surface to promote water collection, while in ref. 55 and 71, low surface energy coatings were applied to the condensation surface (as shown in Fig. 3a and c and 5c). Khanmohammadi *et al.*[81] used plasma coating technology to modify the surface of a glass cover, and experiments found that the contact angle with droplets increased after modification, enhancing the surface hydrophobicity. Moreover, the authors conducted comparative experiments on solar evaporation and water collection using hydrophobic-modified and unmodified glass covers as condensation surfaces (Fig. 6e). The results indicated that the freshwater output of the evaporation system increased by 25.7% after ion coating, significantly improving water collection efficiency. In contrast to the aforementioned homogeneous modification of the entire condensation surface, Sabri *et al.*[82] proposed a mixed wettability surface method to improve water collection efficiency, where part of the condensation surface is hydrophobically modified and the other part remains hydrophilic (Fig. 6f). This design utilizes the hydrophilic surface to promote droplet nucleation, accelerating the condensation rate, while the hydrophobic surface speeds up droplet detachment, increasing the renewal rate of the condensation surface, thereby enhancing water collection efficiency. The study also explored the impact of different modification areas on water collection efficiency and found that when the coated surface area reached 30%, the freshwater production was maximized; excessive low surface energy coatings could increase light reflection, reducing the light absorption capacity of the photothermal material.

Dropwise condensation boosts condensation heat transfer but faces durability challenges in industrial use. For SDIE systems, achieving stable DWC alongside efficient heat conduction is key to ensuring water production efficiency. Traditional polymer coatings (like fluorinated acrylics and parylene), which are low-cost and effective at lowering surface energy, typically range in thickness from 10 nm to 10 μm. Thicker coatings enhance durability. However, due to their low thermal conductivity ($K \approx 0.1$–$1$ W m$^{-1}$ K$^{-1}$), it is essential to minimize coating thickness to cut thermal resistance.[83,84] Yet studies show coatings thinner than 5 μm are prone to pinholes, causing blistering and delamination during condensation and triggering a shift to FWC, which undermines durability.[85] A promising solution to improve polymer coating durability is eliminating pinholes. For instance, conformal deposition techniques[86] or dynamic network-based self-healing polymers[87] can significantly prolong DWC stability.

Ion implantation injects ions like $N^+$, $Cr^+$, and $Ar^+$ into the substrate surface, forming an amorphous alloy layer about 1 nm thick. This reduces surface energy without adding thermal resistance, offering high thermal conductivity and excellent durability. Such coatings can maintain stable dropwise condensation (DWC) for over 15 600 hours, as reported.[88] However, the high material costs limit their use on large-scale condensation surfaces like solar distiller tops. Self-assembled monolayers (SAMs), with their minimal 1–2 nm thickness and negligible thermal resistance, show strong adhesion on copper or gold substrates and have maintained DWC for nine months in reports.[89,90] Yet, SAMs are prone to molecular desorption in steamy environments, challenging their long-term stability and scalability. Beyond coating delamination, the condensation environment also significantly impacts surface performance stability. Volatile organic compounds (VOCs) and diverse microorganisms in seawater pose extra durability challenges for SDIE system condensation surfaces. VOCs can be absorbed by droplets during condensation and act as preferential heterogeneous nucleation sites, disrupting DWC maintenance. Bacterial adhesion can lead to biofilm formation, reducing heat transfer efficiency and potentially impacting water quality. These complex real-world factors highlight the urgent need for enhanced durability of condensation surfaces in SDIE systems.

Upon examining the current strategies for water collection in solar evaporators, it becomes evident that straightforward and cost-effective alterations to the wettability of condensation surfaces to expedite droplet nucleation and detachment constitute an efficient approach to accelerating steam condensation. Such modifications to condensation surfaces are not only facile to implement but also highly adaptable, presenting substantial potential for application within the realm of solar interfacial evaporation. While surface modifications do entail additional costs, it is crucial to keep these expenses to a minimum, all the while augmenting the system's ability to collect water.

To sum up, Table 1 provides a comprehensive overview of rapid vapor condensation strategies in solar evaporation processes and their performance over recent years. Numerous researchers have meticulously engineered photothermal conversion systems, allowing many solar evaporation systems to exceed the theoretical thermal limit of 1.47 kg m$^{-2}$ h$^{-1}$. However, due to constraints in condensation capabilities, the solar to water efficiency and outdoor water production performance are still relatively low. Thus, it is not advisable to rely solely on increasing evaporation rates to boost water production capacity. Given the challenges that current SDIE systems face in enhancing water production capabilities, future research and development strategies should concentrate on creating low-cost and efficient composite condensation systems. These systems are designed to optimize the condensation process through innovative design and material selection, breaking through existing technological barriers. On another note, the dynamic variations in outdoor light intensity, influenced by regional differences and weather changes, make comparing the water production performance of different studies quite challenging. Hence, the adoption of the NWPR (kg kW$^{-1}$ h$^{-1}$

$m^{-2}$) proposed by Cheng *et al.*[70] to characterize water production capacity under outdoor conditions is encouraged. This method offers a more unified and comparable benchmark for evaluating the performance of various SDIE systems in practical applications. The recyclability of SDIE evaporative materials represents another critical focus for future research. For instance, most synthetic hydrogels, such as those based on PAAm or PEG, are neither renewable nor readily biodegradable after their service life, posing a potential risk of microplastic pollution. However, if materials are designed to degrade, this may compromise the long-term stability of the system—a key trade-off that must be carefully addressed. Future studies should therefore prioritize the development of recyclable or biodegradable hydrogels that minimize end-of-life environmental impact without sacrificing performance. Furthermore, the introduction of comprehensive life cycle assessment (LCA) is essential to evaluate the total environmental footprint, from material synthesis to device disposal, thereby truly validating the sustainability of solar-driven desalination systems. With these comprehensive research endeavors, it is anticipated that significant progress in SDIE technology will be made in the near future, providing innovative solutions to combat the global freshwater scarcity.

## 3 Latent heat recovery

In single-stage systems, the latent heat released during the condensation of water vapor is often dissipated into the atmosphere without being harnessed effectively. Acknowledging the significance of latent heat recovery, multi-stage interfacial evaporation systems have been developed and have attracted extensive research interest.[19,95,96] In these multi-stage configurations, the initial stage is commonly outfitted with photothermal absorption materials that absorb sunlight and transform it into thermal energy, which propels the evaporation of saltwater and the generation of vapor. In this process, the condensation latent heat from the vapor in the first stage is employed not only to induce evaporation in the subsequent stage but also to collect condensate water and recuperate latent heat at the current stage, a cycle that persists until the final stage of the system. Consequently, multi-stage systems markedly boost the water production rate compared to their single-stage counterparts. Within multi-stage systems, vapor is generally transported horizontally or downward, effectively circumventing the light reflection issues stemming from water accumulation on transparent condensation surfaces, thus enhancing the system's light absorption efficiency. It should be noted that in multi-stage systems, while the first stage of interfacial evaporation is directly powered by solar energy, the evaporation in subsequent stages depends on the temperature and pressure differential between the vapor from the upper stage and the saltwater in the lower stage.[35,95,97–100] Given that temperature losses are inherent in the transfer process, the evaporation efficiency tends to diminish as the number of stages increases. Hence, the judicious allocation of water production capacity and costs for each stage is vital for the widespread adoption and practical application of multi-stage devices.

Recognizing the substantial potential for recovering latent heat during steam condensation, multi-stage evaporation devices capable of harnessing this energy have been developed. Zhou *et al.*[101] designed the inaugural multi-stage evaporation system, comprising two stages (Fig. 7a). In the initial stage, a photothermal absorption layer is tightly integrated with a hydrophilic PVA sponge that functions as a water supply layer, transporting saltwater to the evaporation surface. A hydrophobic PVDF-HFP layer is strategically woven onto the sponge's reverse to prevent saltwater bypass. The photothermal layer conveys heat to the water supply layer, and the ensuing steam descends through the hydrophobic membrane to the condensation surface, accomplishing the collection of condensate water and the recovery of latent heat for the first stage. The condensation surface of the first stage is in proximity to the water supply layer of the second stage, supplying heat for its evaporation. Under one sun's illumination, this two-stage system achieved a water collection rate of 1.02 kg $m^{-2}$ $h^{-1}$, a notable enhancement from the 0.727 kg $m^{-2}$ $h^{-1}$ rate of a single-stage system. Furthermore, during a 9 hour outdoor water production experiment on a cloudy day, the system yielded a total of 3.67 kg $m^{-2}$ of water. By recuperating the latent heat of steam, this two-stage evaporation structure effectively amplified the overall water production, underscoring the significant potential of multi-stage evaporation in seawater desalination. Asinari *et al.*[102] delved deeper into the correlation between the number of stages and water production in multi-stage systems (Fig. 7b). The findings revealed that, due to the limitations in temperature and pressure differentials between the first and last stages, there is no direct proportionality between the number of stages and water output. While the three-stage configuration of this system produced approximately three times more water than the single-stage setup, the ten-stage configuration only managed six times the output of the single-stage setup. This suggests that there are diminishing returns in increasing the overall number of stages with respect to boosting total water production. At a light intensity of 900 W $m^{-2}$, the ten-stage configuration achieved a total water production of 3 kg $m^{-2}$ $h^{-1}$, demonstrating exceptional water production performance. Given that the salt concentration in the water supply layer increases over the course of the day, potentially leading to a decrease in water production rate and blockage of the evaporation device due to oversaturation, the researchers proposed a salt-resistance strategy involving high water level backwashing of the water supply layer at night to ensure the evaporation system operates efficiently during the day. Due to the meticulous design of the structural parameters of the multi-stage device, the water production efficiency of the ten-stage evaporation device crafted by Wang[98] saw a significant enhancement (Fig. 7c). The condensation plate of the final

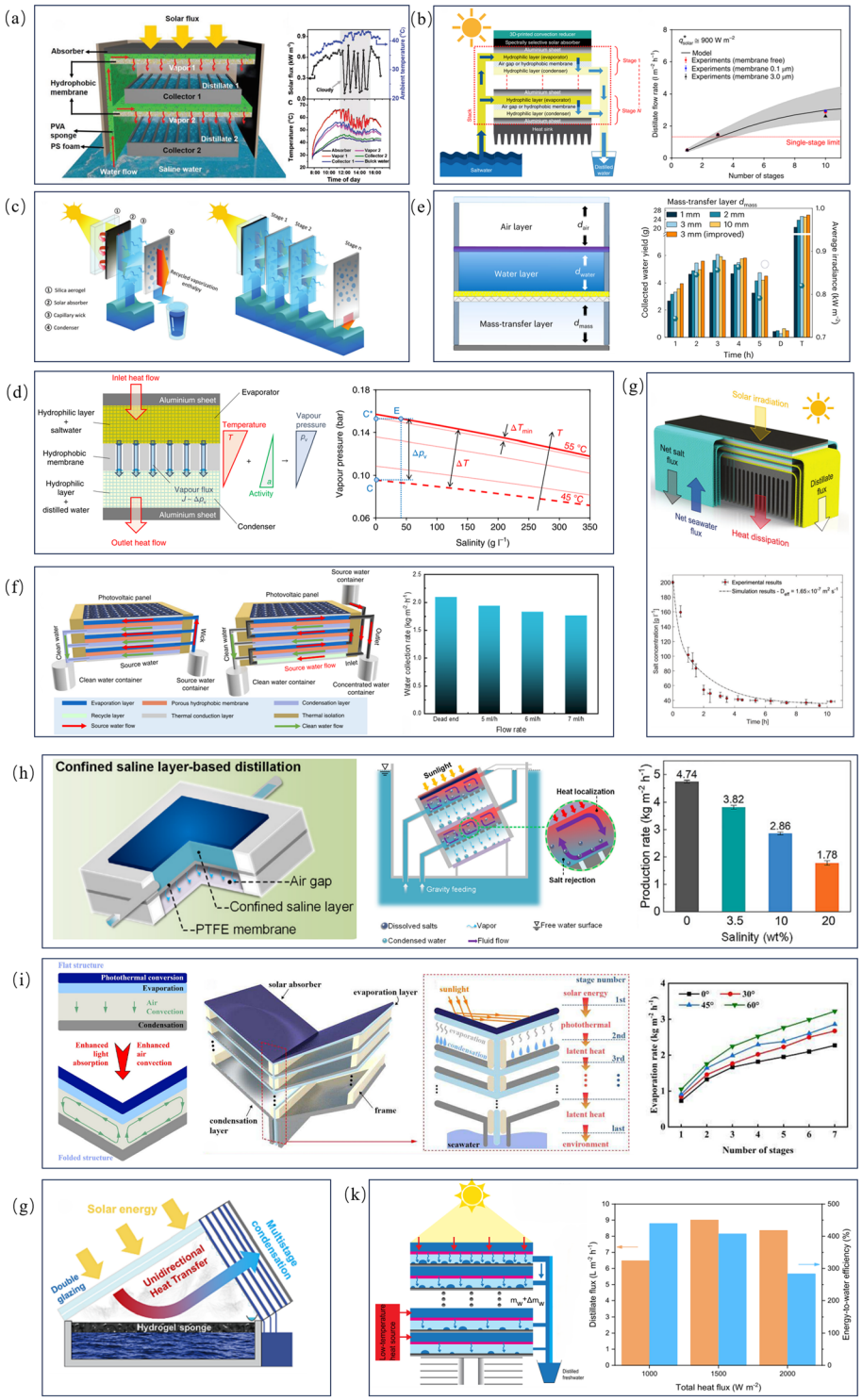


**Fig. 7** a) Schematic diagram of a two-stage solar desalination unit, and outdoor water harvesting performance under cloudy weather;[101] b) solar-powered multistage evaporation unit, and total water harvesting at different number of stages;[102] c) ten-stage solar evaporation unit, and variation of water harvesting at different number of stages;[98] d) the relationship between vapor flux and vapor pressure gradient in a single-stage distiller, as well as the relationship between vapor pressure and the salinity and temperature of water;[102] e) the distance between the layers of each distillation unit and the optimal mass transfer layer distance;[103] f) three-stage solar evaporation unit classified into dead-end and cross-flow modes, and comparison of water harvesting in the two modes;[99] g) three-stage solar evaporation device used to verify the Marangoni effect;[100] h) salt resistance and water harvesting performance of the thermohaline convection-enhanced solar evaporation system;[35] i) multi-stage evaporation system with three-dimensional folded structure, water collection capacity at different number of stages;[104] g) multi-stage evaporation system combined with hydrogel photothermal material, outdoor water collection capacity of the device;[105] k) schematic diagram of improving the performance of a multi-stage evaporation system by heating the condenser, water collection performance of a multi-stage evaporation system at different heat injections.[108]

stage is in direct contact with bulk water, serving as a heat sink to maintain a substantial temperature gradient between stages. This ten-stage configuration achieved a total water production of 5.78 kg $m^{-2}$ $h^{-1}$ under one sun illumination, with the first three stages accounting for 45% of the total water output. The device, which also lacks a specialized salt-resistance method, is designed for daytime operation, employing a mode of operation that prevents the accumulation of high-concentration saltwater in the water supply layer through the automatic diffusion of saltwater at night. The total water production of a multi-stage system is closely related to the thermal resistance between stages, which consists primarily of conductive thermal resistance from physical spacing (*e.g.*, air gaps, hydrophobic membranes) and phase-change resistance during mass transfer. As concluded by Asinari,[102] the vapor flux at each stage is proportional to the vapor pressure gradient across that stage. This gradient results from the competing effects of temperature and salinity gradients (Fig. 7d). Therefore, a certain amount of interstage thermal resistance is necessary to maintain the temperature difference. On the other hand, excessively high thermal resistance limits the heat flux, restricting evaporation and condensation rates at each stage and ultimately constraining the overall system's water production performance. In the work of Xiong *et al.*,[103] the interstage thermal resistance was explicitly modeled to include conduction through the mass transfer layer thickness $d_{mass}$ and sidewall heat losses, among other components (Fig. 7e). Through theoretical and experimental analysis, they found that $d_{mass}$ is a key factor controlling the interstage thermal resistance. There exists an optimal mass transfer layer thickness that maximizes efficiency. For a ten-stage device, the optimal thickness decreases from 3 mm (for a single stage) to 1 mm. This is because, as the number of stages increases, the available temperature difference per stage decreases, necessitating lower thermal resistance to ensure sufficient heat flux. This finding directly corroborates that interstage thermal resistance is a central variable in system design.

In practical multi-stage evaporator operations, the continuous increase in seawater salinity creates a salinity gradient. This leads to salt accumulation and crystallization at the evaporation interface, significantly raising the risk of interface blockage. Such salt-blocking phenomena hinder effective water vapor diffusion, severely restricting the evaporator's long-term stable operation. Consequently, achieving excellent salt-resistance has become a crucial technological challenge that multi-stage evaporators must overcome to progress toward engineering applications. To bolster the performance of multi-stage evaporators under high-salinity conditions, Wang *et al.*[99] engineered a three-stage solar membrane distillation device capable of operating in both dead-end and cross-flow modes, contingent upon the water supply flow pattern (Fig. 7f). In the dead-end mode, saltwater is conveyed to the water supply layer *via* capillary action, a straightforward and viable design that may encounter long-term challenges such as escalating salt concentration and accumulation within the water supply layer, akin to the issues faced by Asinari[102] and Wang.[98] Conversely, the cross-flow mode employs gravity or pumps to remove saltwater from the system prior to saturation, thereby mitigating the salt accumulation associated with prolonged operation, albeit with a minor loss of sensible heat. This design achieved a water production rate of 2.08 kg $m^{-2}$ $h^{-1}$ in dead-end mode and a peak rate of 1.93 kg $m^{-2}$ $h^{-1}$ in cross-flow mode. Asinari *et al.*[100] suggested harnessing the Marangoni effect to augment the convection of salt solutions, thereby enhancing salt resistance, and confirmed the efficacy of this approach in bolstering salt resistance and water production efficiency with a self-made three-stage solar evaporation device (Fig. 7g). Outdoor water production experiments demonstrated that under irradiation below one sun intensity, the water production rate of this three-stage system reached about 2 kg $m^{-2}$ $h^{-1}$. Xu *et al.*[35] introduced an innovative method by confining a thin layer of saltwater between a hydrophobic membrane and a photothermal material, maintaining a consistent liquid level within the system to ensure a steady water supply, thus replacing the hydrophilic materials traditionally utilized in multi-stage setups (Fig. 7h). During operation, heat is transferred from the photothermal material to the enclosed thin layer of saltwater, propelling the saltwater to evaporate through the hydrophobic membrane. The temperature and salt concentration disparities create a density gradient within the enclosed saltwater layer, and by appropriately tilting the device, a thermohaline convection effect is initiated, generating circulation within the sealed saltwater layer and significantly enhancing heat and mass transfer, thereby markedly improving the system's salt resistance and water production capabilities. The water production rates in pure water, 3.5% saltwater, 10% saltwater, and 20% saltwater were as high as 4.74, 3.82, 2.86, and 1.78 kg $m^{-2}$ $h^{-1}$, respectively. Xiong's team[103] proposed a water layer-based reverse evaporation method akin to Xu's[35] design, the core concept of which is to employ head-driven water supply—a thin layer of saltwater—instead of the passive water supply by hydrophilic materials to intensify convection and enhance the system's salt resistance and water production capabilities.

To enhance the water production rate and stability of solar evaporation systems, researchers have not only focused on improving the system's salt-resistance capabilities but also optimized the structure of multi-stage evaporation systems to enhance overall water production performance. Cheng *et al.*[104] proposed an innovative folded multi-stage evaporation structure aimed at strengthening the diffusion of steam (Fig. 7i). Compared to traditional planar structures, this three-dimensional folded structure not only has superior light absorption capabilities but also significantly enhances the convection between the evaporation surface and the condensation surface, increasing the average speed of steam by three orders of magnitude. By adjusting the folding angle

to optimize water production performance, experimental results showed that under single sun illumination, the seven-stage folded evaporation system designed by the team achieved a water production rate of 3.22 kg $m^{-2}$ $h^{-1}$, and it could stably operate even in 20% concentrated saltwater. Gu *et al.*[105] designed a structurally simple new type of multi-stage evaporation device, the innovation of which lies in the integration of hydrogel materials that can reduce the enthalpy of evaporation with multi-stage evaporation modules (Fig. 7j). Using the high-efficiency evaporation

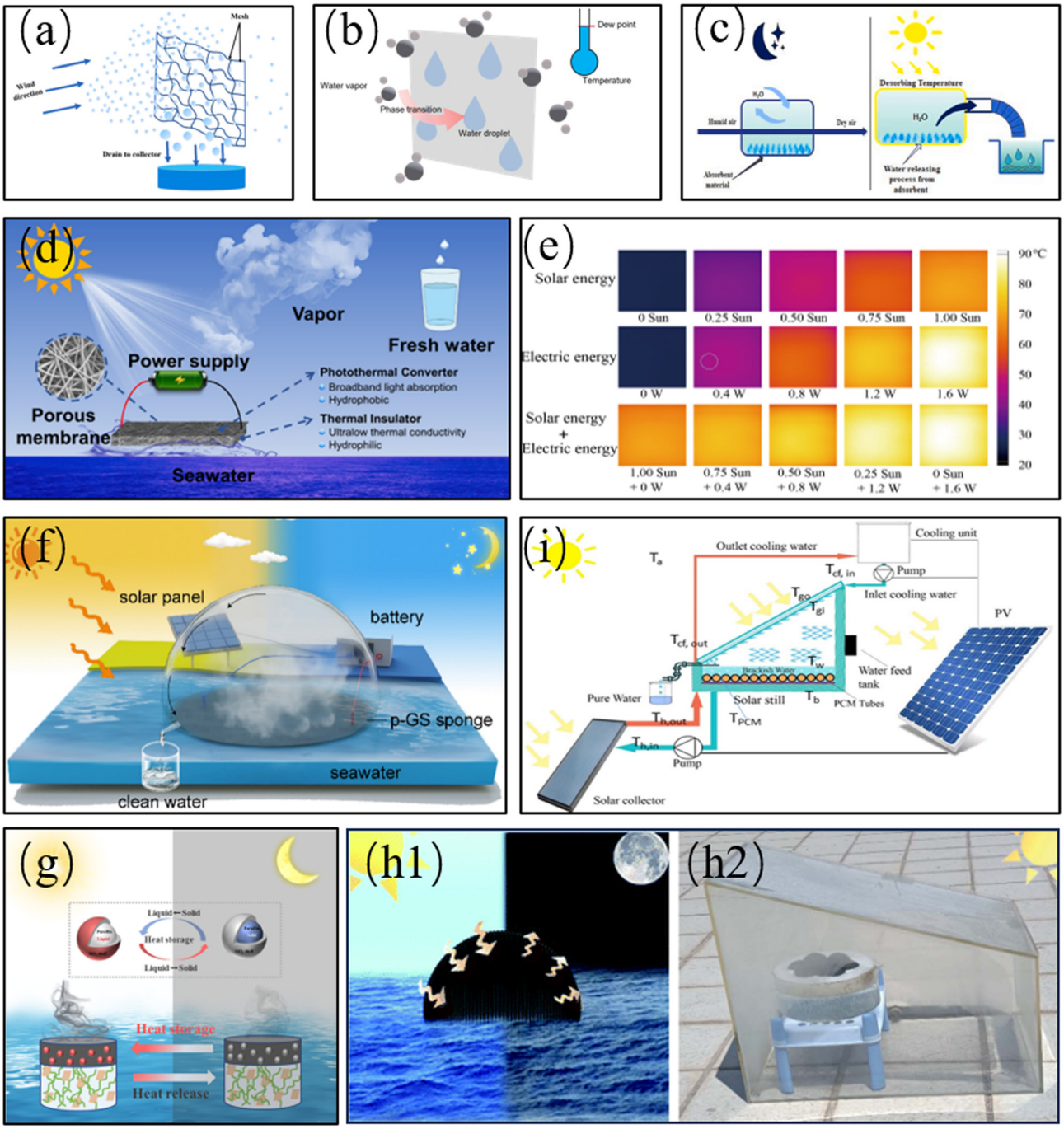


**Fig. 8** a) Schematic of fog collection;[117] b) schematic of dew collection; c) atmospheric water harvesting using adsorbent materials;[117] d) photo-electrothermal joule heating-enhanced water production performance of $Ti_4O_7$ nanofiber membranes;[141] e) comparison of surface temperatures of membranes under different power levels of joule heating *versus* pure photothermal heating;[130] f) the p-GS sponge with photothermal and electrothermal effects for efficient interfacial solar evaporation;[43] g) integrated phase change microcapsules into a double-layered aerogel for enhanced night-time evaporation rate;[135] h1) the Cppy-O evaporator enabling continuous all-day evaporation;[136] h2) outdoor setup for all-day water production using the integrated Cppy-O evaporator;[136] i) solar distillation system combining an external solar collector with phase change materials.[137]

performance of hydrogel photothermal materials to generate a large amount of steam, and by setting up a multi-stage evaporation module on the side of the device without photothermal materials and directly configuring a condensation surface, a directed flow of steam and a continuous multi-stage condensation process were achieved. Due to the introduction of hydrogel materials, the freshwater production of the first stage of the system was significantly improved. Outdoor test results showed that under an average light intensity of 1070 W $m^{-2}$, the total water production rate of this ten-stage system reached 4.5 kg $m^{-2}$ $h^{-1}$. This design effectively combines hydrogel materials commonly used in single-stage solar evaporation with multi-stage evaporation systems, significantly increasing the water production rate and paving a new way for the application of high-performance evaporation materials in multi-stage configurations. In multi-stage evaporation systems, the evaporation driving force of each stage usually comes from the temperature and pressure difference between two stages, so it is common to maintain a lower temperature at the last stage, and a common practice is to set up an effective heat sink at the last stage.[35,100,102,106,107] Wang *et al.*[108] believed that the distillation rate between two stages depends on the transmission of wet steam from the high-temperature side to the low-temperature side, and a lower temperature would result in a reduced maximum content of steam in the air, thereby weakening the system's water production rate. Therefore, they designed the condensation layer in the reverse direction, enhancing the temperature and pressure gradient between stages by increasing the surface temperature of the last two condensers, thereby enhancing the steam transmission rate (Fig. 7k). Under single sun illumination, when an additional heat flux density of 250 W $m^{-2}$ was injected (a total heat flux density of 1500 W $m^{-2}$), the water production reached 9 kg $m^{-2}$ $h^{-1}$, much higher than the 6.5 kg $m^{-2}$ $h^{-1}$ without additional energy injection. However, when a heat flux density of 500 W $m^{-2}$ was injected (a total heat flux density of 2000 W $m^{-2}$), the water production slightly decreased to 8.4 kg $m^{-2}$ $h^{-1}$. This indicates that reasonably heating the last-stage condenser can increase the system's total water production rate. The study proposed a new reverse design principle for the condenser of multi-stage evaporation systems, significantly enhancing the system's water production capacity while not requiring high temperatures for the input heat, providing new possibilities for the reuse of industrial low-temperature waste heat and waste heat.

Multi-stage evaporation systems, capable of recovering latent heat, significantly surpass single-stage systems in water production performance. Moreover, these systems can incorporate strategies for rapid steam condensation, such as modifying condensation surfaces[98,109] or employing advanced condenser structures, thereby further enhancing their water production capabilities. However, most performance evaluations of multi-stage evaporation systems are conducted under high light intensity in clear weather, lacking long-term stability data under variable weather or diverse climatic conditions. The feasibility of employing solar multi-stage evaporation systems as a reliable water source still requires further validation.[19,35,96,103–105,108,110,111]

## 4 All-day water production strategies

The integration of all-weather water production strategies into solar interfacial distillation systems is of significant importance for achieving continuous freshwater supply under conditions of insufficient sunlight or overcast weather. Specifically, all-weather systems are designed to maintain stable and efficient freshwater production even during nighttime or under low solar irradiation conditions such as cloudy days. One major strategy involves coupling atmospheric water harvesting (AWH) technologies with conventional solar stills,[116,117] including fog collection,[118] dew collection,[71,72] and sorption-based atmospheric water capture.[119–122] These approaches share the common goal of extracting moisture from the air and converting it into liquid water under low-light or dark conditions. As illustrated in Fig. 8a, fog collection relies on the collision of fog droplets with the collector surface to achieve water vapor enrichment. A typical fog collector consists of a fine mesh structure that captures suspended micro-droplets in the air, with collected water channeled into a storage unit *via* gravity. This method is highly dependent on environmental conditions and is mostly suitable for high-humidity regions such as mountainous areas. In contrast, dew collection exhibits broader geographical applicability. Dew formation requires the condensing surface to be cooler than the dew point of the air to facilitate phase change condensation (Fig. 8b). For condensation to occur, water molecules must overcome an energy barrier arising from the newly formed interfaces when a liquid nucleus appears. Therefore, hydrophobic modification of the condensing surface can effectively reduce the nucleation energy barrier, thereby enhancing water collection efficiency. Compared to the two methods above, sorbent-based atmospheric water harvesting enables moisture capture and release even at relatively low humidity levels. The working principle is shown in Fig. 8c: hygroscopic materials adsorb atmospheric moisture during the night, and then release it through a solar-driven thermal desorption process during daytime. The released vapor is subsequently condensed into liquid water. Sorbent materials are crucial to AWH systems, as they fundamentally determine the efficiency of water extraction from the atmosphere. Ideal adsorbent materials should possess high adsorption capacity, fast adsorption/desorption kinetics, and good cycling stability. Promising examples reported in the literature include metal–organic frameworks (MOFs),[123] covalent organic frameworks (COFs),[124] hygroscopic salt-based composites,[125,126] and polymeric hydrogels.[122] However, the practical water production capacity remains limited by the adsorbent loading mass and ambient conditions. Although atmospheric water harvesting is operationally simple and widely

applicable, its water production strongly depends on environmental temperature and relative humidity. Overall, the productivity of such systems remains relatively low to date.

Photo-electrothermal Joule heating is another measure to intensify the evaporation rate and can be integrated into solar distillation systems as an all-day water production strategy.[43,127,128] In SDIE systems, photo-electrothermal Joule heating can maintain the system's evaporation and water production functions by providing thermal energy through electrical input to the absorber during nighttime or when sunlight is insufficient. The advantage of this method is its independence from solar energy, enabling water production at any time. Qiu *et al.*[129] developed a novel $Ti_4O_7$ nanofiber membrane with synergistic photothermal and electrothermal effects. *Via* interfacial engineering, they rendered the membrane surface hydrophobic and added a thermal insulation layer at the membrane bottom, optimizing photothermal conversion and thermal management (Fig. 8d). This self-floating bilayer membrane achieved an evaporation rate of 1.86 kg $m^{-2}$ $h^{-1}$ under 1 kW $m^{-2}$ sunlight. With 3 V electrical assistance, the rate increased to 7.51 kg $m^{-2}$ $h^{-1}$, demonstrating excellent all-weather operability. Similarly, Huang *et al.*[130] designed a trilayer composite membrane comprising PVDF, MWCNT, and PDMS layers for a self-heated membrane distillation (SHMD) system. Experiments showed that joule heating outperformed pure photothermal heating in temperature rise rate and final temperature. At 0.25 sun, the membrane surface reached 38.5 °C, whereas with 0.4 W electrical input, joule heating raised it to 71.6 °C (Fig. 8e). This structure effectively combined photothermal and joule heating mechanisms, enhancing system stability and water production. Despite significant progress in boosting evaporation efficiency and stability, further increasing evaporation rates while reducing energy consumption remains a key challenge. Liu *et al.*[131] proposed a biomass-derived porous carbon (MPC)-based artificial blackbody device for high-speed interfacial evaporation *via* low-voltage input. The experimental setup, a modular model using graphite electrodes and MPC as joule heaters, assembled multiple MPC units in a PTFE mold. Direct contact between MPC and a thin water layer in the mold confined the heat, minimizing loss. Results showed an evaporation rate of 98.7 kg $m^{-2}$ $h^{-1}$ at 9 V, surpassing natural evaporation (0.224 kg $m^{-2}$ $h^{-1}$) and conventional photothermal evaporation. In practical applications, all-weather operation and anti-salinity capabilities are also crucial. Zhang *et al.*[43] utilized a Janus-structured graphene@silicone sponge (p-GS sponge), combining photothermal and electrothermal effects, to develop an efficient and salt-resistant interfacial evaporator. The experimental setup included an integrated enclosed device for water collection *via* interfacial evaporation, incorporating the p-GS sponge to drive evaporation through photothermal and electrothermal effects (Fig. 8f). At 1 sun and 5 V from a solar cell, the evaporation rate reached 6.53 kg $m^{-2}$ $h^{-1}$, and even in darkness, it remained at 1.51 kg $m^{-2}$ $h^{-1}$. This study demonstrates that material design and optimization of energy conversion mechanisms can significantly enhance all-weather operation and anti-salinity performance.

The third strategy involves integrating phase change materials (PCMs) into solar stills. PCMs can absorb solar energy and store it as thermal energy during the day and release this energy during nighttime or when sunlight is lacking, supporting the distillation process. This characteristic makes PCMs an ideal choice for enhancing the water production capability of solar stills during non-sunlight hours. During the day, PCMs absorb and store solar energy, and at night, they gradually release the stored heat, providing the necessary thermal energy for the distillation process, thus enabling continuous freshwater supply.[132–134] As shown in Fig. 8g, Guo *et al.*[135] designed a bilayer aerogel structure based on molybdenum disulfide/montmorillonite ($MoS_2$/MMT). The upper layer incorporates paraffin@$SiO_2$ phase change microcapsules (latent heat: 177.85 J $g^{-1}$) for photothermal conversion and thermal storage, while the lower layer consists of MMT aerogel, which is responsible for water supply and thermal insulation. Experiments demonstrated that under 1 kW $m^{-2}$ irradiation, the evaporator achieved an evaporation rate of 1.32 kg $m^{-2}$ $h^{-1}$ with an efficiency of 86.22%. Even after 20 minutes without illumination, it maintained an evaporation rate of 0.71 kg $m^{-2}$ $h^{-1}$ and an efficiency of 44.36%, which is approximately 1.89 times higher than that of the control group without phase change materials during nighttime operation, significantly outperforming evaporators without phase change microcapsules. Similarly, aiming to enhance the efficiency and all-weather operational capability of solar evaporation systems, Geng *et al.*[136] proposed an all-weather solar interfacial evaporator. This evaporator uses polypyrrole-impregnated nylon thread (PNT) as the photothermal layer and an octadecane/carbonized polypyrrole nanotube aerogel composite as the photothermal energy storage unit (Fig. 8h1). Under 1 kW $m^{-2}$ solar irradiation, the evaporator exhibited a high evaporation rate of 2.62 kg $m^{-2}$ $h^{-1}$ with an efficiency of 92.7%. Benefiting from the internal phase change energy storage material, experimental results obtained with a self-built outdoor device (Fig. 8h2) showed that the evaporator could produce 8.42 L $m^{-2}$ of water during the daytime and 1.22 L $m^{-2}$ at night, achieving continuous evaporation around the clock. Furthermore, Al-Harahsheh *et al.*[137] investigated a solar distillation system integrated with an external solar collector and phase change materials (PCMs), using sodium salts (STP, SAT) and paraffin (PWAX) as PCMs (Fig. 8i). Experimental data from May indicated that the daily water production using only the solar still (SS) was 2.1 L $m^{-2}$, while the combination of the solar still with an external solar collector (SSC) significantly increased the output to 9.7 L $m^{-2}$. When PCM was further incorporated into the system, forming the SSCP mode, the productivity increased by nearly 400% compared to the SS mode. These

studies consistently demonstrate that the incorporation of phase change materials significantly enhances the energy utilization efficiency and nighttime continuous water production capacity of solar evaporation systems.

The implementation of these strategies will undoubtedly significantly expand the application scope of solar stills and enhance their operational efficiency. In addition to improving water collection capabilities, multi-stage systems also show great potential in water-electricity cogeneration[19,95,96,111,114,138] and water-salt cogeneration,[106,107,109,110,139,140] providing new directions for increasing the overall resource output rate of solar evaporation systems.

# 5 Light concentration

Typically, the water production capacity of solar interfacial distillation systems is closely related to the limited incident light intensity, which is primarily influenced by various external factors such as altitude, weather conditions, and atmospheric transparency.[142,143] For instance, under cloudy conditions, the incident light intensity diminishes, significantly reducing the water production capability. To address this issue, researchers have proposed a series of concentration methods aimed at enhancing the heat flux of SDIE and have achieved certain results. The principles behind the enhancement of SDIE water production performance through light concentration can be summarized in two points: first, after solar energy is concentrated, the heat flux used for interfacial evaporation increases, which directly raises the evaporation flux and is undoubtedly beneficial for boosting water production.[144–147] Second, due to the increased heat flux density input to the evaporation interface, the temperature of the evaporation surface will significantly increase, meaning that the temperature of the steam will also rise accordingly. This increases the temperature difference between the steam and the external environment (or condensation surface), thereby enhancing the condensation rate of the steam.[35,103] For multi-stage systems, the increased temperature difference between the steam and the heat sink will strengthen the evaporation and condensation driving force at each level, significantly enhancing the overall system's water production capacity.[113,115] Currently, light concentration is achieved by using planar mirrors or high concentration ratio parabolic mirrors to focus light on the photothermal material surface of SDIE. After photothermal conversion, the heat flux density of the distillation system is substantially increased.

For instance, during cloudy conditions, the intensity of incident light decreases, which significantly diminishes the capability for water production. To tackle this challenge, researchers have introduced a variety of concentration techniques to boost the heat flux of SDIE, achieving notable outcomes. The enhancement of SDIE water production performance through light concentration is based on two key principles: firstly, once solar energy is concentrated, the heat flux directed towards interfacial evaporation rises, which directly amplifies the evaporation flux and is unequivocally advantageous for water production.[144–147] Secondly, the increased heat flux density at the evaporation interface leads to a substantial increase in the temperature of the evaporation surface, consequently elevating the temperature of the steam. This amplifies the temperature gradient between the steam and the external environment (or condensation surface), thereby augmenting the steam's condensation rate.[35,103] In multi-stage systems, this heightened temperature differential between the steam and the heat sink intensifies the driving force for evaporation and condensation at each stage, markedly enhancing the system's overall water production capacity.[35,103] Presently, light concentration is executed by utilizing planar mirrors or high concentration ratio parabolic mirrors to direct light onto the photothermal material surface of SDIE. Post-conversion, the heat flux density of the distillation system is considerably heightened.

Deng *et al.*[148] have harnessed an automatic sun-tracking mirror concentrator system for a single-stage SDIE, as depicted in Fig. 9a. This concentrator system, positioned above the evaporation device, is composed of two components: a light reflection system and a sun-tracking mechanism. The light reflection system, made up of four flat mirrors, is engineered to direct sunlight onto the evaporation surface coated with photothermal materials. The sun-tracking system employs photo-sensitive sensors that detect changes in light intensity, adjusting the direction and angle of the reflectors to automatically track the sun's path. This concentrator system's ingenious design has led to a remarkable increase in radiation on the photothermal material surface by 80% under concentrated conditions, and a corresponding boost in the evaporation rate of approximately 68.3% under one sun illumination. The temperature of the absorber surface also saw a rise from 50.2 °C to 62.8 °C. In an outdoor water production experiment spanning from 10 a.m. to 8 p.m., the device impressively yielded 16.867 kg $m^{-2}$ of water. Contrasting with parabolic mirrors that focus light to a single point, flat mirrors lack inherent concentrating properties; thus, to amplify the total radiation, a substantial area of flat mirrors is required to reflect sunlight.[149] This requirement results in limited portability for the entire system and certain constraints on the temperature increase at the evaporation surface.[148,150,151] Consequently, parabolic concentrators with high concentration ratios have been integrated into SDIE. Huang *et al.*[152] leveraged a ring Fresnel solar concentrator, boasting a concentration ratio of up to 62.4, in conjunction with circular Fresnel lenses, to direct sunlight onto the photothermal material surface of a single-stage SDIE device, significantly amplifying its water production capacity (Fig. 9b). The device also integrated advanced strategies for expedited steam condensation, including forced convection *via* a blower and the establishment of subcooled surfaces with additional condensers. Thanks to the high concentration ratios and supplementary condensation tactics,

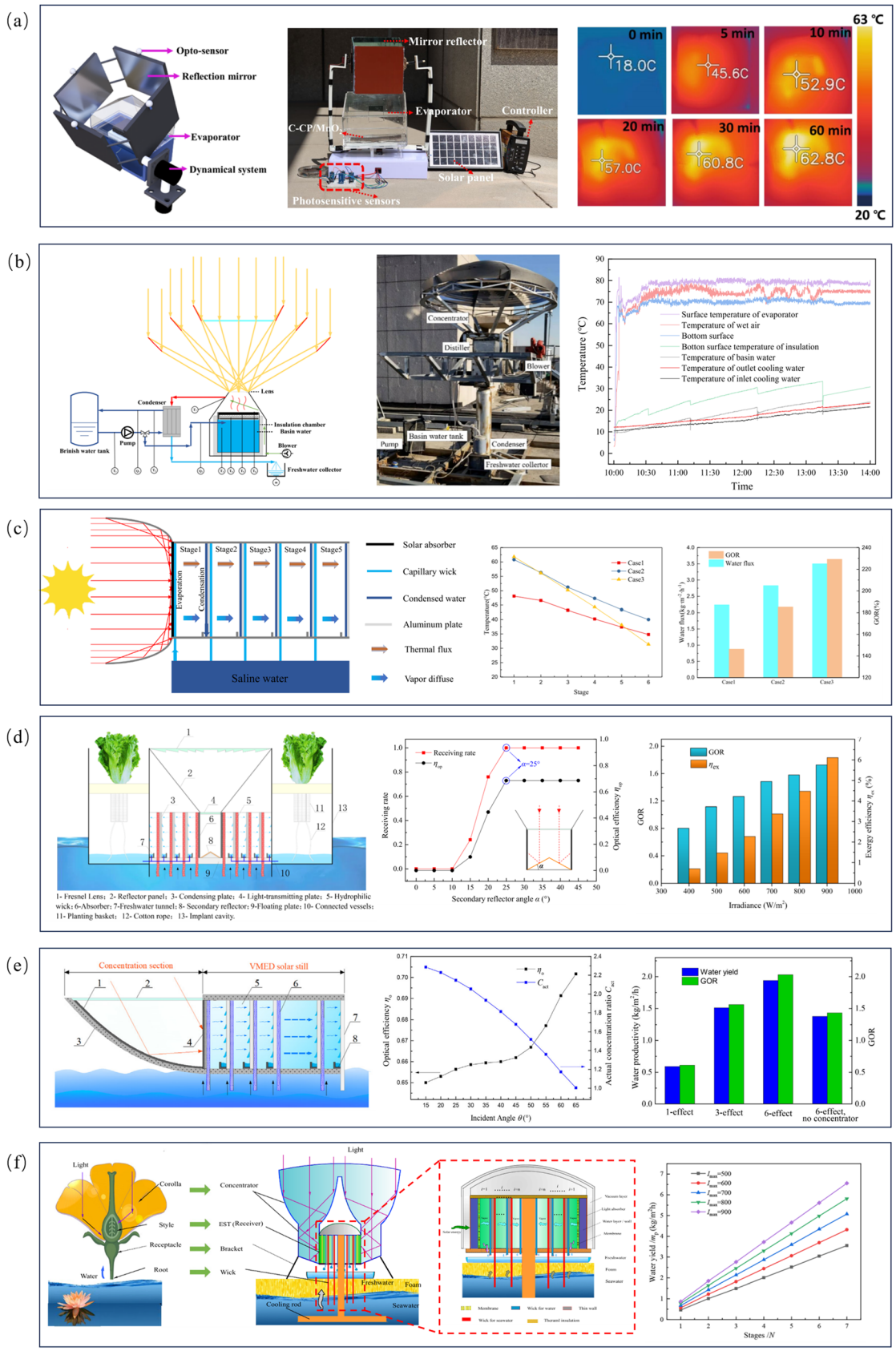


**Fig. 9** a) Planar mirror concentrating solar distillation device with a light-tracking system;[148] b) solar distillation unit with a high-power concentrator;[152] c) five-stage solar steam generation system coupled with a compound parabolic concentrator;[154] d) a floating planting system based on a concentrated solar multi-stage distillation device;[155] e) a parabolic concentrator-coupled multistage solar still with concentrators designed based on local geographic locations;[156] f) bionics-based corolla-shaped concentrator-coupled solar multi-stage distillation device.[157]

the device showcased remarkable water production performance in outdoor trials. Within a mere 4 hours and under natural light intensities varying from 380 to 500 W $m^{-2}$, the device achieved a noteworthy water output of 21.25 kg $m^{-2}$, with an average hourly rate of about 5.3 kg $m^{-2}$, and the absorber surface temperature escalated to 81.53 °C. However, the light-to-water conversion efficiency remained relatively modest at its peak of 27.1%, a consequence of the high concentration ratio and extensive lens area. It's crucial to acknowledge that the increased evaporation flux and uneven concentration heighten the requirements for water transport capacity and the speed of steam condensation; failing to meet these can result in a water production capability that falls short of the potential provided by high-power solar radiation. While this design demonstrated superior water production capabilities, the intricacy of high-concentration device design and the ancillary costs of concentrators are pivotal considerations. Furthermore, the loss of latent heat during the direct condensation of high-temperature steam represents a significant waste of energy. A more substantial temperature differential can foster the creation of a pronounced temperature gradient within the device, thereby enhancing heat and mass transfer processes.[153] Based on this, some researchers have initiated investigations into the application of concentrators in multi-stage systems, aiming to optimize water production rates to their fullest potential. Wei *et al.*[154] have successfully integrated a concentrator system with a multi-stage solar evaporation setup specifically for desalination applications, as illustrated in Fig. 9c. They positioned a truncated compound parabolic concentrator (CPC) along the side of the multi-stage device, which effectively redirected light onto the primary solar absorber, harnessing the power of concentration. Within this concentrated lighting arrangement, the team conducted three comparative experiments that spanned a spectrum of increasing temperature gradients, labeled as case 1, case 2, and case 3. The findings from these experiments revealed that a heightened temperature gradient notably boosted the rates of water production and the efficiencies of solar to water efficiency.

The optical efficiency of a system is defined by the proportion of radiative energy captured by the absorber surface relative to the total solar energy the system receives. To boost this efficiency, certain studies have concentrated on refining the structural design of concentrator devices, aiming to amplify the absorber's energy capture and, by extension, the water production capabilities. In this domain, Zheng's team has achieved significant breakthroughs,[146,147,155–157] culminating in the development of an integrated multi-stage distillation floating cultivation system harnessing concentrated solar energy[155] (Fig. 9d). This innovative system seamlessly integrates a solar concentration system, a four-stage evaporation setup, and a hydroponic system into a single unit. By meticulously adjusting the inclination angle of the reflection panels, the system achieves precise control over the angle of reflected light, optimizing the light path and enhancing optical efficiency. In their study, the optical efficiency peaked at 66% when the secondary reflection panel was angled at 25°. Indoor experiments revealed that under a solar irradiance of 900 W $m^{-2}$, the system could achieve a water production rate of 2.25 kg $m^{-2}$ $h^{-1}$, with an impressive light-to-water conversion efficiency of up to 170%. In the concentrator's design process, it is crucial to take into account the geographical characteristics of the installation site, particularly when designing the geometric contour of the parabolic concentrator based on the minimum annual solar incidence angle, ensuring that all sunlight reflected by the concentrator is efficiently absorbed by the photothermal surface of the multi-stage distiller. Guided by this design philosophy, the team's concentrator, when combined with a solar six-stage distillation device, achieved an average optical efficiency of up to 67%[156] (Fig. 9e). Under an irradiance of 700 W $m^{-2}$, the temperature of the photothermal absorber surface of the device could rise to 87.1 °C, with a water production rate and light-to-water conversion efficiency reaching 1.94 kg $m^{-2}$ $h^{-1}$ and 203%, respectively. In another study by Zheng *et al.*, a novel biomimetic coronet-shaped concentrator was designed[157] (Fig. 9f). The optimization of the concentrator structure enabled a light reception rate of 75% at an incidence angle of 20°. As a result, this seven-stage distillation system with concentrated solar energy showcased exceptional performance, with the photothermal absorber surface temperature nearing 100 °C under an irradiance of 900 W $m^{-2}$, and the water production rate and light-to-water conversion efficiency reaching as high as 6.5 kg $m^{-2}$ $h^{-1}$ and 480%, respectively. The cost of freshwater from concentrated solar evaporation devices is \$1–18 per $m^3$ (Table 3), higher than RO (\$0.45–1.72 per $m^3$), MSF (\$0.52–8 per $m^3$), and MED (\$0.56–1.75 per $m^3$).[158] On the other hand, SDIE technology can operate independently of the electrical grid and fossil fuels, offering irreplaceable value in remote and off-grid areas. It shows strong potential for small-scale, distributed emergency water supply and household-level applications. The future research focus should not be to compete with RO, MSF, or MED on cost, but rather to advance ultra-low-cost materials, design highly efficient condensation systems, and improve operational lifetime and stability—making the technology economically viable within these specific application scenarios.

# 6 Conclusion and prospect

SDIE, with its eco-friendly and versatile advantages, holds significant promise for tackling water shortages. Despite this, refining water production strategies is a central challenge. The implementation of rapid steam condensation, latent heat recovery, and light concentration has notably improved the water production and energy efficiency of solar interfacial evaporation systems.

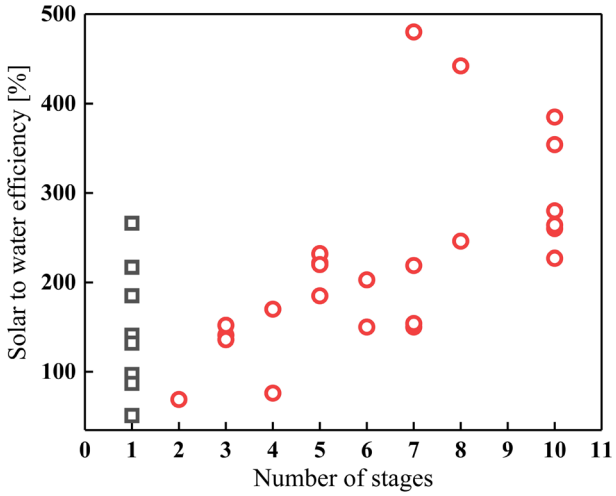


Fig. 10 Solar to water efficiency at different stages based on Tables 1–3.

Some single-stage solar distillation systems with rapid steam condensation strategies have matched the water production efficiency of multi-stage systems (Fig. 10), highlighting the importance of rapid condensation in boosting water output. While symmetrical condensation surface designs have improved light absorption and condensation efficiency in single-stage setups, their benefits are limited by issues like light reflection and reduced condensation force. Inverting the structure in single-stage systems can enhance water collection, but the gain is constrained by low evaporation rates. Future research should aim to increase input energy or lower evaporation enthalpy to raise the evaporation rate. Introducing forced convection not only boosts water collection efficiency but also increases total water production by elevating the evaporation rate, though it must account for additional energy use. Harnessing natural wind energy could mitigate this issue. Additionally, creating sub-ambient temperature condensation surfaces can enhance condensation force, but the cooling system's reverse design is crucial, as lower temperatures do not invariably equate to higher water production efficiency. Modifying condensation surfaces is a broadly applicable method to strengthen condensation in solar distillation systems, with significant implications for water collection efficiency. Future studies should concentrate on optimizing and integrating these strategies to develop more efficient and economical solar distillation systems.

Table 2 Summary of water production performance of multistage solar evaporation systems

| Materials | | | | Total stage number | Light intensity W $m^{-2}$ | WPR kg $m^{-2}$ $h^{-1}$ | Solar to water efficiency % | Ref. |
|---|---|---|---|---|---|---|---|---|
| Solar absorbance | Water supply layer | Vapor diffusion layer | Condenser | | | | | |
| ~95% | PVA sponge | PVDF-HFP nanofibers | Multi-fin aluminum plate | 2 | 1000 | 1.02 | 69 | 101 |
| 85% | Cotton layer | PTFE membranes | Aluminum plate | 4 | 1000 | 1.11 | 76 | 111 |
| ~86% | Hydrophilic quartz glass fibrous membrane | Electrospun porous polystyrene membrane | Hydrophilic quartz glass fibrous membrane | 3 | 1000 | 2.08 (dead-end) 1.93 (cross-flow) | 141 (dead-end) 131 (cross-flow) | 99 |
| ~95% | Synthetic microfiber | Air gap | Aluminum plate | 3 | 950 | 1.9 | 136 | 100 |
| 93% | Air-laid paper | Air gap | Aluminum foil | 7 | 1000 | 2.21 | 150 | 112 |
| 93.5% | Cotton layer | Air gap | Cooper tube | 6 | 1000 | 2.2 | 150 | 113 |
| 95% | Water gap | Air gap | Aluminum plate | 3 | 1000 | 2.23 | 152 | 107 |
| 94.1% | Paper towel | Air gap | Cooper plate | 7 | 1000 | 2.26 | 154 | 114 |
| 98.24% | Air-laid paper | Air gap | Hydrophilic aluminum plate | 7 | 1000 | 3.22 | 219 | 104 |
| 89% | Non-woven fabrics | PTFE membranes | Stainless steel mesh | 5 | 750 | 2.45 | 222 | 110 |
| ~95% | Synthetic microfiber | Air gap or PTFE membranes | Aluminum plate | 10 | ~900 | 3 | 227 | 102 |
| 92.4% | Hydrophilic paper | Air gap | Hydrophobic aluminum plate | 5 | 1000 | 3.53 | 232 | 115 |
| 89% | R-paper | Polypropylene membrane | R-paper | 8 | 1000 | 3.61 | 246 | 97 |
| — | Fibrous paper | Air gap | Hydrophobic aluminum plate | 10 | 1070 | 4.5 | 280 | 105 |
| — | Confined saline | PTFE membranes | Aluminum plate | 10 | 1000 | 4.74 (pure water) 3.82 | 322 (pure water) 260 | 35 |
| ~93% | Paper towel | Air gap | Hydrophobic aluminum plate | 10 | 1000 | 5.78 (pure water) | 385 (pure water) | 98 |
| 91.4% | Confined saline | PTFE and PP membranes | Hydrophobic aluminum plate | 10 | 1000 | 5.88 (pure water) 5.20 | 400 (pure water) 354 | 103 |
| 99% | Water gap | Air gap | CNT + FPTS membrane | 8 | 1000 | 6.5 9.0 | 442 408 | 108 |

Table 3 Performance summary of concentrated solar evaporation devices

| Total stage number | Reflector | Concentration ratio | Absorber surface temperature °C | Sunlight intensity W $m^{-2}$ | WPR | Solar to water efficiency % | Production cost | Ref. |
|---|---|---|---|---|---|---|---|---|
| 1 | Flat mirror | — | 62.8 | 0–700 (natural sunlight) | 16.867 kg $m^{-2}$ $d^{-1}$ (10 h) | — | — | 148 |
| 1 | Fresnel solar concentrator | 62.4 | 81.53 | 380–500 (natural sunlight) | 21.25 kg $m^{-2}$ $d^{-1}$ (4 h) | 27.1 | — | 152 |
| 2 | Semicircle concentrator | 2 | 50 | 606 (natural sunlight) | 4.45 kg $m^{-2}$ $d^{-1}$ (6 h) | — | \$18 per $m^3$ | 153 |
| 5 | CPC concentrator | 2 | 60.799 | 1000 | 2.82 kg $m^{-2}$ $h^{-1}$ | 185.09 | \$7.03 per $m^3$ | 154 |
| 4 | Fresnel solar concentrator | 1.75 | 56.2 | 900 | 2.25 kg $m^{-2}$ $h^{-1}$ | 170 | \$15 per $m^3$ | 155 |
| 6 | Parabolic concentrator | 2.29 | 87.1 | 700 | 1.94 kg $m^{-2}$ $h^{-1}$ | 203 | \$12.47 per $m^3$ | 156 |
| 7 | Corolla-shaped concentrator | 2.92 | 100 | 900 | 6.5 kg $m^{-2}$ $h^{-1}$ | 480 | \$1 per $m^3$ | 157 |
| 5 | Parabolic concentrator | 2.3 | 83 | 900 | 2.7 kg $m^{-2}$ $h^{-1}$ | 220 | — | 146 |
| 10 | Fresnel solar concentrator | — | 72 | 1000 | 3.98 kg $m^{-2}$ $h^{-1}$ | 264 | \$13 per $m^3$ | 147 |

Multi-stage evaporation systems, with their ability to recover latent heat, substantially outperform single-stage solar stills in water production capacity. To further enhance the performance of solar distillation systems, future efforts can focus on the following areas: (i) as observed from Table 3, many multi-stage systems use fibrous materials like hydrophilic paper for water supply. These materials have a relatively low evaporation rate compared to those that can reduce evaporation enthalpy. Utilizing such materials in the initial or any stage of a multi-stage setup could be beneficial, given that latent heat can be recovered. (ii) Innovative approaches to rapid steam condensation should be explored, such as employing forced convection to boost evaporation and condensation, or creating subcooled surfaces at the final heat sink to increase the driving force. Techniques like light concentration or electric fields to elevate the evaporation temperature of the first stage, thereby increasing the overall temperature gradient and driving force, are also worth considering. (iii) Leveraging phase change materials or joule heating for all-weather water production strategies can be integrated into multi-stage systems to capitalize on low light intensity steam, thereby enhancing water production. (iv) Light concentration technology, which not only amplifies the system's energy input but also establishes a larger temperature gradient, is a cost-effective method to enhance water production. It is crucial to address potential issues like uneven photothermal material surface temperatures due to refracted light spots, necessitating rapid water transport materials or advanced salt resistance measures. By refining and integrating these strategies, the efficiency and water production capacity of multi-stage interfacial evaporation systems can be significantly improved, offering more viable solutions for practical applications.

The advancement of water production strategies in SDIE confronts unresolved common issues that impede progress. First, fluctuations in outdoor light intensity complicate the correlation between absorbed solar energy and water output across various experiments, hindering effective performance comparisons between studies. Thus, standardizing performance metrics under consistent solar input is crucial. Second, to bolster the commercial viability of SDIE technology, considerations of investment, operational costs, and return on investment are essential, particularly for systems incorporating additional energy sources or components like concentrators. Lastly, integrating water and electricity co-production, along with water and salt recovery—especially the extraction of valuable metals like lithium from marine resources—enhances the resource yield of solar distillation systems, boosting their economic and resource utilization efficiency. Addressing these issues systematically, standardizing performance metrics, and refining economic models are vital for advancing solar interfacial evaporation technology towards practical, efficient, and commercially viable solutions.

## Conflicts of interest

There are no conflicts to declare.

## Data availability

The data that support the findings of this study are available from the corresponding author upon reasonable request.

## Acknowledgements

This work was supported by the National Key Research and Development Program of China (No. 2022YFD2100402), Tianjin Continuing Education Teaching Reform and Quality Improvement Research Program Project (No. J202313).

## References

1 F. Dolan, *et al.*, Evaluating the economic impact of water scarcity in a changing world, *Nat. Commun.*, 2021, **12**(1), 1915.

2 F. Morante-Carballo, *et al.*, What Do We Know about Water Scarcity in Semi-Arid Zones? A Global Analysis and Research Trends, *Water*, 2022, **14**(17), 2685.
3 B. Nazari and M. Keshavarz, Water population density: Global and regional analysis, *Theor. Appl. Climatol.*, 2023, **153**(1), 431–445.
4 WMO, *New water and climate coalition launched ahead of World Water Day*.
5 Z. Ai, F. Ishihama and N. Hanasaki, Mapping Current and Future Seawater Desalination Plants Globally Using Species Distribution Models, *Water Resour. Res.*, 2022, **58**(7), 2021WR031156.
6 E. Jones, *et al.*, The state of desalination and brine production: A global outlook, *Sci. Total Environ.*, 2019, **657**, 1343–1356.
7 M. M. Mekonnen and A. Y. Hoekstra, Four billion people facing severe water scarcity, *Sci. Adv.*, 2016, **2**(2), 1500323.
8 W. Leal Filho, *et al.*, Understanding responses to climate-related water scarcity in Africa, *Sci. Total Environ.*, 2022, **806**, 150420.
9 M. Salehi, Global water shortage and potable water safety; Today's concern and tomorrow's crisis, *Environ. Int.*, 2022, **158**, 106936.
10 W. Ba, *et al.*, Urban water scarcity in China: A systematic review of research advances and future directions, *Appl. Geogr.*, 2023, **159**, 103069.
11 C. He, *et al.*, Future global urban water scarcity and potential solutions, *Nat. Commun.*, 2021, **12**(1), 4667.
12 M. Kummu, *et al.*, The world's road to water scarcity: shortage and stress in the 20th century and pathways towards sustainability, *Sci. Rep.*, 2016, **6**(1), 38495.
13 P. Talebbeydokhti, *et al.*, Analysis and optimization of LT-MED system powered by an innovative CSP plant, *Desalination*, 2017, **413**, 223–233.
14 J. Leblanc and J. Andrews, Low-Temperature Multi-Effect Evaporation Desalination Systems Coupled with Salinity-Gradient Solar Ponds, *Int. J. Energy Res.*, 2009, 2151–2157.
15 A. A. Tareemi and S. W. Sharshir, A state-of-art overview of multi-stage flash desalination and water treatment: Principles, challenges, and heat recovery in hybrid systems, *Sol. Energy*, 2023, **266**, 112157.
16 M. Elimelech and W. A. J. S. Phillip, The Future of Seawater Desalination: Energy, Technology, and the Environment, *Science*, 2011, **333**, 712–717.
17 M. Qasim, *et al.*, Reverse osmosis desalination: A state-of-the-art review, *Desalination*, 2019, **459**, 59–104.
18 Y. J. Lim, *et al.*, Seawater desalination by reverse osmosis: Current development and future challenges in membrane fabrication – A review, *J. Membr. Sci.*, 2021, **629**, 119292.
19 Z. Mao, *et al.*, High Performance Solar-Driven Power-Water Cogeneration for Practical Application: From Micro/Nano Materials to Beyond, *ACS Nano*, 2024, **18**(34), 22648–22663.
20 P. Zhang, *et al.*, Boosting the Viable Water Harvesting in Solar Vapor Generation: From Interfacial Engineering to Devices Design, *Adv. Mater.*, 2024, **36**(5), e2303976.
21 H. Ghasemi, *et al.*, Solar steam generation by heat localization, *Nat. Commun.*, 2014, **5**(1), 4449.
22 X. Wu, *et al.*, Interfacial Solar Evaporation: From Fundamental Research to Applications, *Adv. Mater.*, 2024, **36**(23), e2313090.
23 Y. Lin, *et al.*, Solar steam generation based on the photothermal effect: from designs to applications, and beyond, *J. Mater. Chem. A*, 2019, **7**, 19203–19227.
24 X. Li, *et al.*, Measuring Conversion Efficiency of Solar Vapor Generation, *Joule*, 2019, **3**(8), 1798–1803.
25 A. H. Elsheikh, *et al.*, Thin film technology for solar steam generation: A new dawn, *Sol. Energy*, 2019, **177**, 561–575.
26 D. Zhu, *et al.*, Efficient degradation of tetracycline by RGO@black titanium dioxide nanofluid via enhanced catalysis and photothermal conversion, *Sci. Total Environ.*, 2021, **787**, 147536.
27 Y. Guo, *et al.*, Biomass-Derived Hybrid Hydrogel Evaporators for Cost-Effective Solar Water Purification, *Adv. Mater.*, 2020, **32**(11), 1907061.
28 X. Zhou, *et al.*, Architecting highly hydratable polymer networks to tune the water state for solar water purification, *Sci. Adv.*, 2019, **5**(6), eaaw5484.
29 B. Yang, *et al.*, Flatband lambda-Ti(3)O(5) towards extraordinary solar steam generation, *Nature*, 2023, **622**(7983), 499–506.
30 Q. Zhao, *et al.*, Low vaporization enthalpy hydrogels for highly efficient solar-driven interfacial evaporation, *Desalination*, 2023, **568**, 116999.
31 J. Sun, *et al.*, Minimizing enthalpy of evaporation in solar steam generation: An emerging strategy beyond theoretical evaporation limitation, *Mater. Today*, 2024, 619–647.
32 J. Yan, *et al.*, Spatial Confinement Engineered Gel Composite Evaporators for Efficient Solar Steam Generation, *Adv. Sci.*, 2024, **11**(41), e2407295.
33 X. Li, *et al.*, Three-dimensional artificial transpiration for efficient solar waste-water treatment, *Natl. Sci. Rev.*, 2018, **5**(1), 70–77.
34 P. Zhang, *et al.*, Three-dimensional water evaporation on a macroporous vertically aligned graphene pillar array under one sun, *J. Mater. Chem. A*, 2018, **6**(31), 15303–15309.
35 J. Gao, *et al.*, Extreme salt-resisting multistage solar distillation with thermohaline convection, *Joule*, 2023, **7**(10), 2274–2290.
36 P. Tao, *et al.*, Solar-driven interfacial evaporation, *Nat. Energy*, 2018, **3**(12), 1031–1041.
37 Y. Wang, *et al.*, Thermo-adaptive interfacial solar evaporation enhanced by dynamic water gating, *Nat. Commun.*, 2024, **15**(1), 6157.
38 C. Li, *et al.*, A Covalent Organic Framework/Graphene Dual-Region Hydrogel for Enhanced Solar-Driven Water Generation, *J. Am. Chem. Soc.*, 2022, **144**(7), 3083–3090.
39 Y. Yang, *et al.*, A general salt-resistant hydrophilic/hydrophobic nanoporous double layer design for efficient and stable solar water evaporation distillation, *Mater. Horiz.*, 2018, **5**(6), 1143–1150.
40 M. Gao, *et al.*, Solar absorber material and system designs for photothermal water vaporization towards clean water

and energy production, *Energy Environ. Sci.*, 2019, **12**(3), 841–864.
41 Z. Yu, *et al.*, Enhanced Interfacial Solar Evaporation through Formation of Micro-Meniscuses and Microdroplets to Reduce Evaporation Enthalpy, *Adv. Funct. Mater.*, 2022, **32**(17), 2108586.
42 L. Zhang, *et al.*, Hydrophobic Light-to-Heat Conversion Membranes with Self-Healing Ability for Interfacial Solar Heating, *Adv. Mater.*, 2015, **27**(33), 4889–4894.
43 L. Li and J. Zhang, Highly salt-resistant and all-weather solar-driven interfacial evaporators with photothermal and electrothermal effects based on Janus graphene@silicone sponges, *Nano Energy*, 2021, **81**, 105682.
44 Y. Guo, *et al.*, Tailoring Nanoscale Surface Topography of Hydrogel for Efficient Solar Vapor Generation, *Nano Lett.*, 2019, **19**(4), 2530–2536.
45 H. Liang, *et al.*, Thermal Efficiency of Solar Steam Generation Approaching 100% through Capillary Water Transport, *Angew. Chem., Int. Ed.*, 2019, **58**(52), 19041–19046.
46 G. Ni, *et al.*, A salt-rejecting floating solar still for low-cost desalination, *Energy Environ. Sci.*, 2018, **11**(6), 1510–1519.
47 J. Ren, *et al.*, Hofmeister effect mediated hydrogel evaporator for simultaneous solar evaporation and thermoelectric power generation, *Chem. Eng. J.*, 2023, **458**, 141511.
48 L. Chen, *et al.*, Cost-effective, scalable fabrication of self-floating xerogel foam for simultaneous photothermal water evaporation and thermoelectric power generation, *Chem. Eng. J.*, 2023, **454**, 140383.
49 L. Hao, *et al.*, High-performance solar-driven interfacial evaporation through molecular design of antibacterial, biomass-derived hydrogels, *J. Colloid Interface Sci.*, 2022, **608**, 840–852.
50 J. Qian, *et al.*, Ice templated and ice seed tailored hydrogels for highly efficient solar evaporator, *Desalination*, 2024, **575**, 117292.
51 Y. Wang and D. Wu, Regulating the evaporation surface architecture of anisotropic chitosan hydrogels for high-efficiency solar desalination, *J. Mater. Chem. A*, 2024, **12**(7), 4099–4107.
52 C. Pan, *et al.*, Optimization of Evaporation and Condensation Architectures for Solar-Driven Interfacial Evaporation Desalination, *Membranes*, 2022, **12**(9), 899.
53 F. Wang, *et al.*, A high-performing single-stage invert-structured solar water purifier through enhanced absorption and condensation, *Joule*, 2021, **5**(6), 1602–1612.
54 F. Yu, *et al.*, Molybdenum Carbide/Carbon-Based Chitosan Hydrogel as an Effective Solar Water Evaporation Accelerator, *ACS Sustainable Chem. Eng.*, 2020, **8**(18), 7139–7149.
55 H. Yao, *et al.*, Janus-interface engineering boosting solar steam towards high-efficiency water collection, *Energy Environ. Sci.*, 2021, **14**(10), 5330–5338.
56 J. Li, *et al.*, Over 10 kg m−2 h−1 Evaporation Rate Enabled by a 3D Interconnected Porous Carbon Foam, *Joule*, 2020, **4**(4), 928–937.
57 Y. Wang, *et al.*, Same materials, bigger output: A reversibly transformable 2D–3D photothermal evaporator for highly efficient solar steam generation, *Nano Energy*, 2021, **79**, 105477.
58 N. Li, *et al.*, Solar-Driven Interfacial Evaporation and Self-Powered Water Wave Detection Based on an All-Cellulose Monolithic Design, *Adv. Funct. Mater.*, 2021, **31**(7), 2008681.
59 J. R. Welty, C. E. Wicks and R. E. Wilson, *Fundamentals of momentum, heat, and mass transfer*, 1969.
60 H. Lu, *et al.*, High-Yield and Low-Cost Solar Water Purification via Hydrogel-Based Membrane Distillation, *Adv. Funct. Mater.*, 2021, **31**(19), 2101036.
61 C. Ma, *et al.*, Biomimetic Hybridization of Janus-like Graphene Oxide into Hierarchical Porous Hydrogels for Improved Mechanical Properties and Efficient Solar Desalination Devices, *ACS Nano*, 2021, **15**(12), 19877–19887.
62 X. Liu, *et al.*, Evaporation rate far beyond the input solar energy limit enabled by introducing convective flow, *Chem. Eng. J.*, 2022, **429**, 132335.
63 J. Li, *et al.*, Ultrahigh solar vapor evaporation rate of super-hydrophilic aerogel by introducing environmental energy and convective flow, *Chem. Eng. J.*, 2023, **466**, 143281.
64 B. Wang, *et al.*, Solar interfacial evaporation systems with multi-field synergies boost water purification and blue energy harvesting technologies, *Energy Environ. Sci.*, 2024, **17**(20), 7600–7626.
65 C. Zhang, *et al.*, Distinct stage-wise environmental energy harvesting behaviors within solar-driven interfacial water evaporation coupled with convective airflow, *Nano Energy*, 2023, **107**, 108142.
66 H. W. Lim, H. Seung Lee and S. Joon Lee, Laminated chitosan/graphene nanoplatelets aerogel for 3D interfacial solar desalination with harnessing wind energy, *Chem. Eng. J.*, 2024, **480**, 148197.
67 F. Liu, *et al.*, Low Cost, Robust, Environmentally Friendly Geopolymer–Mesoporous Carbon Composites for Efficient Solar Powered Steam Generation, *Adv. Funct. Mater.*, 2018, **28**(47), 1803266.
68 W. Sun, *et al.*, Enhancing freshwater production with a high-performance solar interface evaporator and in low-vacuum environment: A solar-driven low-vacuum interfacial distillation system, *Desalination*, 2023, **568**, 117014.
69 W. Li, *et al.*, Portable Low-Pressure Solar Steaming-Collection Unisystem with Polypyrrole Origamis, *Adv. Mater.*, 2019, **31**(29), e1900720.
70 Z. Yu, *et al.*, Micro-Nano Water Film Enabled High-Performance Interfacial Solar Evaporation, *Nano-Micro Lett.*, 2023, **15**(1), 214.
71 Z. Xi, *et al.*, All-Day Freshwater Harvesting by Selective Solar Absorption and Radiative Cooling, *ACS Appl. Mater. Interfaces*, 2022, **14**(22), 26255–26263.
72 L. Wei, H. S. Soo and Z. Chen, Patterned Hybrid Surfaces for Efficient Dew Harvesting, *ACS Appl. Mater. Interfaces*, 2024, **16**(38), 51715–51726.
73 Z. Zhu, *et al.*, Understanding the effect of the condensation temperature on solar-driven reverse distillation for

enhanced water production, *Energy Convers. Manage.*, 2024, **301**, 118024.
74 R. Wen, *et al.*, Sustaining enhanced condensation on hierarchical mesh-covered surfaces, *Natl. Sci. Rev.*, 2018, **5**(6), 878–887.
75 S. Zhang, *et al.*, The effect of surface-free energy and microstructure on the condensation mechanism of water vapor, *Prog. Nat. Sci.: Mater. Int.*, 2023, **33**(1), 37–46.
76 S.-F. Zheng, U. Gross and X.-D. Wang, Dropwise condensation: From fundamentals of wetting, nucleation, and droplet mobility to performance improvement by advanced functional surfaces, *Adv. Colloid Interface Sci.*, 2021, **295**, 102503.
77 X. Lan, *et al.*, Enhancing the vapor condensation efficiency of a solar water purifier by rapid heat dissipation to bottom bulk water, *J. Mater. Chem. A*, 2022, **10**(21), 11784–11792.
78 M. Javed, *et al.*, Complete System to Generate Clean Water from a Contaminated Water Body by a Handmade Flower-like Light Absorber, *ACS Omega*, 2021, **6**(50), 35104–35111.
79 L. Wei, *et al.*, Water vapor condensation behavior on different wetting surfaces via molecular dynamics simulation, *Surf. Interfaces*, 2024, **52**, 104981.
80 C. Dang, *et al.*, Structure integration and architecture of solar-driven interfacial desalination from miniaturization designs to industrial applications, *Nat. Water*, 2024, **2**(2), 115–126.
81 S. Khanmohammadi and S. Khanjani, Experimental study to improve the performance of solar still desalination by hydrophobic condensation surface using cold plasma technology, *Sustain. Energy Technol. Assess.*, 2021, **45**, 101129.
82 N. M. Shatar, *et al.*, Mix wettability surface on solar still cover for freshwater productivity enhancement, *Desalination*, 2022, **534**, 115797.
83 K. M. Holden, *et al.*, The Use of Organic Coatings to Promote Dropwise Condensation of Steam, *J. Heat Transfer*, 1987, **109**(3), 768–774.
84 P. J. Marto, *et al.*, Evaluation of organic coatings for the promotion of dropwise condensation of steam, *Int. J. Heat Mass Transfer*, 1986, **29**(8), 1109–1117.
85 J. Ma, *et al.*, Condensation Induced Delamination of Nanoscale Hydrophobic Films, *Adv. Funct. Mater.*, 2019, **29**(43), 1905222.
86 A. T. Paxson, *et al.*, Stable Dropwise Condensation for Enhancing Heat Transfer via the Initiated Chemical Vapor Deposition (iCVD) of Grafted Polymer Films, *Adv. Mater.*, 2014, **26**(3), 418–423.
87 B. B. Jing and C. M. Evans, Catalyst-Free Dynamic Networks for Recyclable, Self-Healing Solid Polymer Electrolytes, *J. Am. Chem. Soc.*, 2019, **141**(48), 18932–18937.
88 Y. C. Guo and Z. X. Wang, *Amorphous Physics*, Science Press, Beijing, China, 1984.
89 I. Orkan, Droplet condensation on polymer surfaces: A review, *Turk. J. Chem.*, 2013, **37**, 643–674.
90 D. Schroeder-Richter, S. Yildiz and G. Bartsch, Effect of porous coating on critical heat flux, *Int. Commun. Heat Mass Transfer*, 1996, **23**(4), 463–471.
91 Z. Wang, M. Elimelech and S. Lin, Environmental Applications of Interfacial Materials with Special Wettability, *Environ. Sci. Technol.*, 2016, **50**(5), 2132–2150.
92 Q. Zhang, *et al.*, Vertically Aligned Janus MXene-Based Aerogels for Solar Desalination with High Efficiency and Salt Resistance, *ACS Nano*, 2019, **13**(11), 13196–13207.
93 J. Qian, *et al.*, Ice templated and ice seed tailored hydrogels for highly efficient solar evaporator, *Desalination*, 2024, **575**, 117292.
94 L. Hao, *et al.*, High-performance solar-driven interfacial evaporation through molecular design of antibacterial, biomass-derived hydrogels, *J. Colloid Interface Sci.*, 2022, **608**(Pt 1), 840–852.
95 N. A. S. Elminshawy, *et al.*, A novel concentrated photovoltaic-driven membrane distillation hybrid system for the simultaneous production of electricity and potable water, *Renewable Energy*, 2020, **162**, 802–817.
96 M. Ebrahimian, *et al.*, All-in-One Hybrid Solar-Driven Interfacial Evaporators for Cogeneration of Clean Water and Electricity, *Adv. Funct. Mater.*, 2024, 2412870.
97 W. Wang, *et al.*, Solar Seawater Distillation by Flexible and Fully Passive Multistage Membrane Distillation, *Nano Lett.*, 2021, **21**(12), 5068–5074.
98 Z. Xu, *et al.*, Ultrahigh-efficiency desalination via a thermally-localized multistage solar still, *Energy Environ. Sci.*, 2020, **13**(3), 830–839.
99 W. Wang, *et al.*, Simultaneous production of fresh water and electricity via multistage solar photovoltaic membrane distillation, *Nat. Commun.*, 2019, **10**(1), 3012.
100 M. Morciano, *et al.*, Solar passive distiller with high productivity and Marangoni effect-driven salt rejection, *Energy Environ. Sci.*, 2020, **13**(10), 3646–3655.
101 G. Xue, *et al.*, Highly Efficient Water Harvesting with Optimized Solar Thermal Membrane Distillation Device, *Glob. Chall.*, 2018, **2**(5–6), 1800001.
102 E. Chiavazzo, *et al.*, Passive solar high-yield seawater desalination by modular and low-cost distillation, *Nat. Sustain.*, 2018, **1**(12), 763–772.
103 Z. Zhu, *et al.*, Passive solar desalination towards high efficiency and salt rejection via a reverse-evaporating water layer of millimetre-scale thickness, *Nat. Water*, 2023, **1**(9), 790–799.
104 Y. Li, *et al.*, A three-dimensional folded multistage distillation device with enhanced air convection for efficient solar interface evaporation, *Desalination*, 2023, **562**, 116714.
105 X. Luo, *et al.*, Ultrahigh freshwater production achieved by unidirectional heat transfer interfacial evaporation solar still integrated with waste heat recovery, *Energy Convers. Manage.*, 2024, **304**, 118226.
106 D. Ghim, *et al.*, Achieving maximum recovery of latent heat in photothermally driven multi-layer stacked membrane distillation, *Nano Energy*, 2021, **80**, 105444.
107 Y. Dong, *et al.*, High-yielding and stable desalination via photothermal membrane distillation with free-flow evaporation channel, *Desalination*, 2022, **543**, 116103.

108 P. Poredos, *et al.*, Ultra-high freshwater production in multistage solar membrane distillation via waste heat injection to condenser, *Nat. Commun.*, 2024, **15**(1), 7890.
109 Y. Tian, *et al.*, Solar-Driven Multistage Device Integrating Dropwise Condensation and Guided Water Transport for Efficient Freshwater and Salt Collection, *Environ. Sci. Technol.*, 2024, **58**(17), 7335–7345.
110 W. Wang, *et al.*, Integrated solar-driven PV cooling and seawater desalination with zero liquid discharge, *Joule*, 2021, **5**(7), 1873–1887.
111 L. Huang, *et al.*, Solar-driven co-generation of electricity and water by evaporation cooling, *Desalination*, 2020, **488**, 114533.
112 Y. Li, *et al.*, Stable, zero liquid discharge, and highly efficient solar-driven multistage distillation device based on tree-inspired radial water transfer, *J. Cleaner Prod.*, 2022, **375**, 134025.
113 L. Huang, *et al.*, Enhanced water yield of solar desalination by thermal concentrated multistage distiller, *Desalination*, 2020, **477**, 114260.
114 B.-L. Bai, *et al.*, A novel solar-driven water and electricity cogeneration integrated system by multistage vaporization enthalpy recycling, *Desalination*, 2022, **542**, 116040.
115 J. Xu, *et al.*, Energy and exergy analysis of a novel solar-powered passive multi-stage osmosis desalination system for sustainable water production, *Energy Convers. Manage.*, 2024, **321**, 119099.
116 C. Lei, *et al.*, Chemistries and materials for atmospheric water harvesting, *Chem. Soc. Rev.*, 2024, **53**(14), 7328–7362.
117 B. Tashtoush and A. Alshoubaki, Atmospheric water harvesting: A review of techniques, performance, renewable energy solutions, and feasibility, *Energy*, 2023, **280**, 128186.
118 Z. Yu, *et al.*, Fog Harvesting Devices Inspired from Single to Multiple Creatures: Current Progress and Future Perspective, *Adv. Funct. Mater.*, 2022, **32**(26), 2200359.
119 X. Zhang, *et al.*, Autonomous Atmospheric Water Harvesting over a Wide RH Range Enabled by Super Hygroscopic Composite Aerogels, *Adv. Mater.*, 2024, **36**(41), 2310219.
120 X. Yang, *et al.*, Enhanced continuous atmospheric water harvesting with scalable hygroscopic gel driven by natural sunlight and wind, *Nat. Commun.*, 2024, **15**(1), 7678.
121 T. Li, *et al.*, Scalable and efficient solar-driven atmospheric water harvesting enabled by bidirectionally aligned and hierarchically structured nanocomposites, *Nat. Water*, 2023, **1**, 971–981.
122 H. Zhou, *et al.*, Solar-Driven Drum-Type Atmospheric Water Harvester Based on Bio-Based Gels with Fast Adsorption/Desorption Kinetics, *Adv. Mater.*, 2024, **36**(32), 2403876.
123 H. Kim, *et al.*, Adsorption-based atmospheric water harvesting device for arid climates, *Nat. Commun.*, 2018, **9**(1), 1191.
124 H. L. Nguyen, Covalent Organic Frameworks for Atmospheric Water Harvesting, *Adv. Mater.*, 2023, **35**(17), 2300018.
125 M. Ejeian, A. Entezari and R. Z. Wang, Solar powered atmospheric water harvesting with enhanced LiCl /MgSO4/ACF composite, *Appl. Therm. Eng.*, 2020, **176**, 115396.
126 M. Elashmawy and I. Alatawi, Atmospheric Water Harvesting from Low-Humid Regions of Hail City in Saudi Arabia, *Nat. Resour. Res.*, 2020, **29**(6), 3689–3700.
127 J. Ma, *et al.*, A solar-electro-thermal evaporation system with high water-production based on a facile integrated evaporator, *J. Mater. Chem. A*, 2020, **8**(41), 21771–21779.
128 L. Cui, *et al.*, High Rate Production of Clean Water Based on the Combined Photo-Electro-Thermal Effect of Graphene Architecture, *Adv. Mater.*, 2018, **30**, 1706805.
129 L. Li and J. Zhang, Highly salt-resistant and all-weather solar-driven interfacial evaporators with photothermal and electrothermal effects based on Janus graphene@silicone sponges, *Nano Energy*, 2021, **81**, 105682.
130 J. Huang, T. Tang and Y. He, Coupling photothermal and Joule-heating conversion for self-heating membrane distillation enhancement, *Appl. Therm. Eng.*, 2021, **199**, 117557.
131 F. Liu, *et al.*, Electrically powered artificial black body for low-voltage high-speed interfacial evaporation, *J. Mater. Chem. A*, 2022, **10**(43), 22992–23000.
132 A. A. Saeed, *et al.*, Improving the drum solar still performance using corrugated drum and nano-based phase change material, *J. Energy Storage*, 2022, **55**, 105647.
133 W. I. A. Aly, M. A. Tolba and M. Abdelmagied, Experimental investigation and performance evaluation of an oval tubular solar still with phase change material, *Appl. Therm. Eng.*, 2023, **221**, 119628.
134 J. Kateshia and V. Lakhera, A comparative study of various fatty acids as phase change material to enhance the freshwater productivity of solar still, *J. Energy Storage*, 2022, **48**, 103947.
135 Q. Guo, *et al.*, Design of MoS2/MMT bi-layered aerogels integrated with phase change materials for sustained and efficient solar desalination, *Desalination*, 2022, **541**, 116028.
136 L. Geng, *et al.*, Interfacial solar evaporator synergistic phase change energy storage for all-day steam generation, *J. Mater. Chem. A*, 2022, **10**(29), 15485–15496.
137 M. Al-Harahsheh, *et al.*, Self-powered solar desalination using solar still enhanced by external solar collector and phase change material, *Appl. Therm. Eng.*, 2022, **206**, 118118.
138 G. Antonetto, *et al.*, Synergistic freshwater and electricity production using passive membrane distillation and waste heat recovered from camouflaged photovoltaic modules, *J. Cleaner Prod.*, 2021, **318**, 128464.
139 Z. Yang, *et al.*, Developing Salt-Rejecting Evaporators for Solar Desalination: A Critical Review, *Environ. Sci. Technol.*, 2024, **58**(20), 8610–8630.
140 Y. Li, *et al.*, Stable, zero liquid discharge, and highly efficient solar-driven multistage distillation device based on tree-inspired radial water transfer, *J. Cleaner Prod.*, 2022, **375**, 134025.
141 X. Qiu, *et al.*, Interface Engineering of a Ti4O7 Nanofibrous Membrane for Efficient Solar-Driven Evaporation, *ACS Appl. Mater. Interfaces*, 2022, **14**(49), 54855–54866.

142 T. Arunkumar, D. Parbat and S. J. Lee, Comprehensive review of advanced desalination technologies for solar-powered all-day, all-weather freshwater harvesting systems, *Renewable Sustainable Energy Rev.*, 2024, **199**, 114505.
143 R. Niu, *et al.*, Bio-Inspired Sandwich-Structured All-Day-Round Solar Evaporator for Synergistic Clean Water and Electricity Generation, *Adv. Energy Mater.*, 2023, **13**, 2302451.
144 L. Wang, *et al.*, Advanced strategies in solar interfacial desalination: Enhancing water productivity and salt resistance, *Chem. Eng. J.*, 2024, **500**, 156563.
145 Y. Chen, *et al.*, Experimental study of electric field enhancing the vapor production of the solar interfacial evaporator, *Renewable Energy*, 2024, **220**, 119663.
146 L. Wang, *et al.*, Experimental investigation on a floating multi-effect solar still with rising seawater film, *Renewable Energy*, 2022, **195**, 194–202.
147 L. Wang, *et al.*, Thermodynamic and economic analysis of a solar hydroponic planting system with multi-stage interfacial distillation units, *Desalination*, 2022, **539**, 115970.
148 S. Wang, *et al.*, Solar Interface Evaporation System Assisted by Mirror Reflection Heat Collection Based on Sunflower Chasing the Sun, *ACS Appl. Mater. Interfaces*, 2022, **14**(39), 44958–44968.
149 C. Zhang, *et al.*, Planar metasurface-based concentrators for solar energy harvest: from theory to engineering, *PhotoniX*, 2022, **3**(1), 28.
150 M.-H. Sun, *et al.*, Three-Dimensional Mirror-Assisted and Concave Pyramid-Shaped Solar–Thermal Steam Generator for Highly Efficient and Stable Water Evaporation and Brine Desalination, *ACS Appl. Mater. Interfaces*, 2023, **15**(22), 27120–27129.
151 F. A. Essa, *et al.*, Enhancement of pyramid solar distiller performance using reflectors, cooling cycle, and dangled cords of wicks, *Desalination*, 2021, **506**, 115019.
152 C. Chen, *et al.*, Experimental analysis of a solar interfacial evaporation under high power concentrator, *Energy*, 2024, **295**, 131064.
153 H. Cheng, *et al.*, A concentrating light multistage rising film solar distiller with a central cooling structure, *Sol. Energy*, 2023, **257**, 96–109.
154 M. Li, *et al.*, An optical concentrator coupled multistage solar steam generation system for solar thermal-latent heat cascade utilization and water desalination: Performance and economic benefit analysis, *Sep. Purif. Technol.*, 2022, **303**, 122191.
155 L. Wang, *et al.*, A floating planting system based on concentrated solar multi-stage rising film distillation process, *Energy Convers. Manage.*, 2022, **254**, 115227.
156 L. Wang, *et al.*, Performance study of a passive vertical multiple-effect diffusion solar still directly heated by parabolic concentrator, *Renewable Energy*, 2022, **182**, 855–866.
157 Y. Zhao, *et al.*, Performance analysis and optimization of a novel high-efficiency flower-inspired solar still, *Energy Convers. Manage.*, 2022, **251**, 114878.
158 A. Al-Karaghouli and L. L. Kazmerski, Energy consumption and water production cost of conventional and renewable-energy-powered desalination processes, *Renewable Sustainable Energy Rev.*, 2013, **24**, 343–356.